TROISIEME CYCLE DE LA PHYSIQUE
EN SUISSE ROMANDE

HIGH ENERGY ASTROPHYSICS I

by

PHILIPPE JETZER

INSTITUT FÜR THEORETISCHE PHYSIK
UNIVERSITÄT ZÜRICH
Winterthurerstrasse 190, 8057 Zürich
SWITZERLAND

SEMESTRE D'HIVER 2003 - 2004

TROISEME CYCLE DE LA PHYSIQUE
EN SUISSE ROMANDE

UNIVERSITES DE :
BERNE - FRIBOURG - GENEVE
LAUSANNE - NEUCHATEL
&
ECOLE POLITECHNIQUE FEDERALE DE LAUSANNE

* * * * * * *

ARCHIVES & VENTE DE POLYCOPIES :
M. D. REYMOND, UNIVERSITE DE LAUSANNE
BATIMENT DES SCIENCES PHYSIQUES
1015 LAUSANNE-DORIGNY

Contents

Introduction

One might define “High-energy astrophysics” as the astrophysics which deals with high-energy processes and their applications in the astrophysical context. The goal of these lectures is to describe the main high-energy processes and their application in astrophysics. This is certainly one of the most exciting areas of modern astrophysical research and involves some of the most difficult problems of contemporary physics. A few examples include the study of massive black holes in active galactic nuclei and the acceleration of high energy particles.

Until 1945 astronomers could only study the Universe in the optical waveband. Since that time there has been an enormous expansion of the wavebands available for astronomical study. The new disciplines of radio, millimeter, infrared, ultraviolet, X and γ-ray astronomy combined with optical astronomy have led to the growth of many new areas of astrophysics. This has been possible thanks to the rapid development of new technologies and the launch of satellites.

For these lectures we will mostly follow the books by Longair [1].

Chapter 1

Historical remarks

1.1 The discovery of cosmic rays

The cosmic rays story begins about 1900 when it was found that electroscopes discharged even if they were kept in the dark well away from sources of natural radioactivity. It was then shown by Rutherford that most of the ionisation was due, however, to natural radioactivity.

In 1910 Wulf performed an experiment on the Eiffel Tower at an height of 330 m using electro-meters. He found that the ionisation fell from $6 \times 10^6\ ions\ m^{-3}$ to $3.5 \times 10^6\ ions\ m^{-3}$ as he ascended the Eiffel Tower. If the ionisation had been due to γ-rays originating at the surface of the Earth, the intensity of the ions should have decreased to half its value within only 80 meters and would have been negligible at the top of the Tower.

A big step forward was made in 1912 and 1913 when first Hess and then Kolhörster made manned balloon ascents in which they measured the ionisation of the atmosphere with increasing altitude ranging from 5 to $9\ Km$. They found that the average ionisation increased with respect to the ionisation at sea-level above about $1.5\ Km$. This is clearly evidence that the source of the ionisation must be extraterrestrial.

From the 1930s to the early 1950s, the cosmic radiations provided a natural source of very high energy particles which were energetic enough to penetrate into the nucleus. This way turned out to be the main technique by which new particles were discovered until the early 1950s:

the positron e^+ in 1932 (Anderson);

the muon μ^- in 1936 (Anderson and Neddermeyer);

the pions $\pi^\pm$ in 1947 (Powell et al.).

Further particles were found in cosmic rays. However, by 1953 the accelerator technology had developed to the point where energies comparable to those available in the cosmic rays could be produced in the laboratory. Accordingly, the interest in cosmic rays shifted to the problems of their origin and their propagation in astrophysical environments from their sources to the Earth [2].

In the region of the energy spectrum which is unaffected by the propagation of the particles to the Earth through the Solar Wind ($E \geq 10^9 eV$), the energy spectra of the cosmic ray particles can be described by

$$N(E) = kE^{-x} \tag{1.1}$$

in the energy range $10^9 - 10^{14} eV$, with $x \approx 2.5 - 2.7$ and k a constant.

This relation is valid for protons, electrons and nuclei, clearly with other values of the constant k. For photons one finds other values for x.

The chemical composition of the cosmic rays is similar to the abundances of the elements in the Sun, with some exceptions, particularly for the light elements which appear to be higher in cosmic rays.

At very high energies cosmic rays are detected by large air shower arrays on the surface of the Earth. Their arrival rate is very low, nevertheless particles with energies up to $10^{20} eV$ and even beyond have been detected.

How high the maximum energy of cosmic rays reaches is one of the most important problems in cosmic rays research. Possible detection of cosmic rays with energies above $10^{20} eV$ has given rise to many discussions regarding their energy.

Indeed, if high energy cosmic rays (protons) come from outside of our galaxy, they interact with cosmic microwave background photons and cannot travel cosmological distances. This interaction causes a cutoff in the energy spectrum near $5 \times 10^{19} eV$ (Greisen-Zatsepin-Kuzmin GKZ cut-off) [3, 4].

The mean free path length is about $20 Mpc$, corresponding to roughly the distance to the nearest cluster of galaxies (Virgo cluster).

If cosmic rays with energies above the GZK cut-off are confirmed then there is the problem to explain their origin. A problem thus which is still open: either the particles get accelerated within our galaxy, but what is the mechanism responsible for it, or there are new particles which decay and give rise to high energy cosmic rays.

1.2 X-ray instruments

X-ray astronomy can only be carried out at very high altitudes because of photoelectric absorption of X-rays by the atoms and molecules of the Earth's atmosphere.

Thus the exploration of the X-ray sky was possible only after rockets flight were possible.

- The full scope of X-ray astronomy became clear in the early 1970s with the launch of the first dedicated X-ray satellite, the **UHURU** satellite Observatory.

- In 1978, the **Einstein** X-ray Observatory was launched. It provided the first high resolution images of many X-ray sources and made very deep surveys

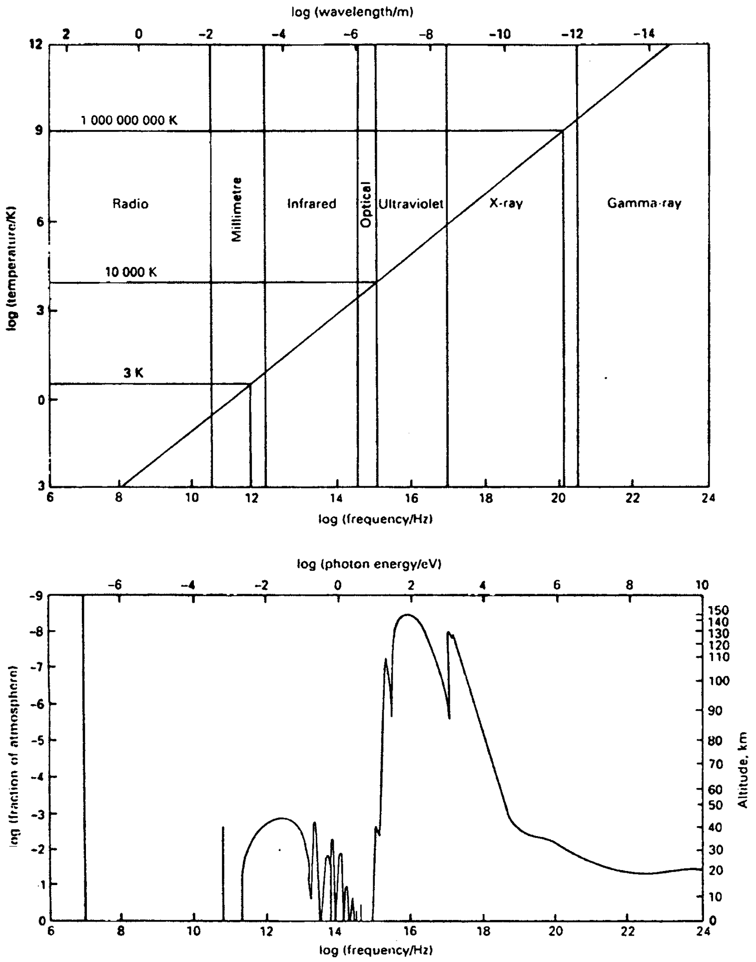

(a)

(b)

Figure 1.1: (a) The relation between the temperature of a black-body and the frequency (or wavelength) at which most of the energy is emitted. The frequency (or wavelength) plotted is that corresponding to the maximum of a black-body at temperature T. Convenient expressions for this relation are:
$\nu_{max} = 10^{11}(T/K)\ Hz; \quad \lambda_{max}T = 3 \times 10^6\ nm\ K$
The ranges of wavelength corresponding to the different wavebands - radio, millimetre, infrared, optical, ultraviolet, X and γ-rays are shown. (b) The transparency of the atmosphere for radiation of different wavelengths. The solid line shows the height above sea-level at which the atmosphere becomes transparent for radiation of different wavelengths. From Ref. [5]

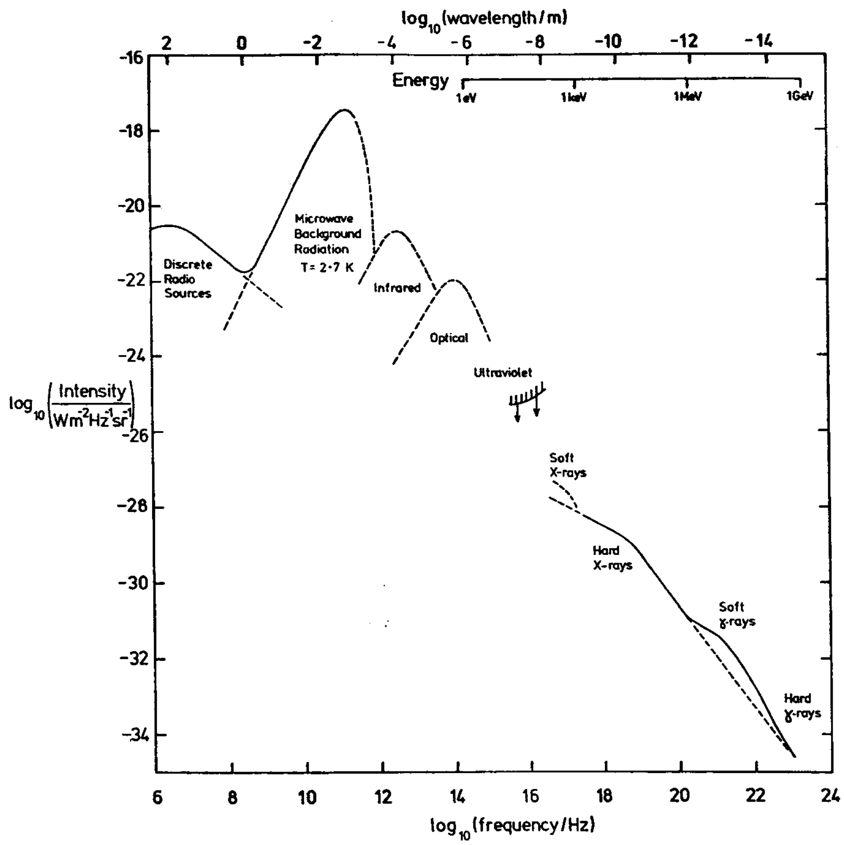

Figure 1.2: The spectrum of an extragalactic background radiation as it was known in 1969 (Longair and Sunyaev 1971). The solid lines indicate regions of the electromagnetic spectrum in which extragalactic background radiation had been measured. The dashed lines were theoretical estimates of the background radiation due to discrete sources and should not be taken very seriously. From Ref. [6]

of small areas of the sky and a first good in sight into the bulk properties of the intracluster plasma in galaxy cluster was provided [7].

- The **ROSAT**, the ROetgen SATellite (turned off, after a long life, on February 12, 1999) provided observations in great detail of the intracluster medium, revealing different forms of interaction of the relativistic and thermal plasma. Other main research goals were studies of the solar system, stars and stellar clusters, compact galactic objects, nearby normal galaxies and active galactic nuclei.

- **ASCA** (the Advanced Satellite for Cosmology and Astrophysics) is Japan's fourth cosmic X-ray astronomy mission. The satellite was successfully launched on February 20, 1993. ASCA is the first X-ray astronomy mission to combine imaging capability with a broad pass band, good spectral resolution and large effective area. The mission also is the first satellite to use CCDs for X-ray astronomy. With these properties, the primary scientific purpose of ASCA was the X-ray spectroscopy of astrophysical plasma-especially the analysis of discrete features such as emission lines and absorption edges. The sensitivity of ASCA's instruments allowed the first detailed, broad-band spectra of distant quasars to be derived. In addition, ASCA's suite of instruments provides the best opportunity so far for identifying the sources whose combined emission makes up the cosmic X-ray background.

- The X-ray satellite **SAX** or **BeppoSAX** (in honour of Giuseppe (Beppo) Occhialini), a program of the Italian Space Agency with participation of the Netherlands Agency for Aerospace Programs, was launched on April 30, 1996 from Cape Canaveral. The payload is characterised by a very wide spectral coverage from 0.1 to 300 keV, with well balanced performances both from its low and high energy instrumentation. Its sensitivity allowed the exploitation of the full band for weak sources, opening new perspectives in the study of spectral shape and variability of several classes of objects. Furthermore, the presence of wide field cameras allowed monitoring of the long term variability of sources and the discovery of X-ray transient phenomena.

  BeppoSAX provided an important contribution in several areas of X-ray astronomy such as:

  - Compact galactic sources: shape and variability of the various continuum components and of the narrow spectral features (e.g. iron line, cyclotron lines); phase resolved spectroscopy. Discovery and study of X-ray transients.
  - Active Galactic Nuclei: spectral shape and variability of the continuum and of the narrow and broad features from 0.1 to 200 keV in bright objects (soft excess, warm and cold absorption and related O and Fe edges, iron line and high energy bump, high energy cut-off);

  - Cluster of galaxies: spatially resolved spectra of nearby objects and the study of temperature gradients; chemical composition and temperature of more distant clusters;
  - Supernova remnants: spatially resolved spectra of extended remnants; spectra of Magellanic Cloud remnants;
  - Gamma-ray bursts: temporal profile with 1 msec resolution from 60 to 600 keV. X-ray counterparts of a subset with positional accuracy of 5'.

- NASA's **CHANDRA** X-ray Observatory, which was launched and deployed by Space Shuttle Columbia in July of 1999, was designed to have three times the area of the Einstein mirror at low energies and to have considerable collecting area between 6 and 7 keV, corresponding to the energy range of iron lines emitted by many astrophysical sources.

  The combination of high resolution, large collecting areas and sensitivity to higher energy X-rays makes it possible for CHANDRA to study extremely faint sources, sometimes strongly absorbed, in crowded fields.

  X-rays from distant clusters of galaxies (which are faint and small) can be imaged and spectra measured as a function of position within the cluster. Furthermore, since clusters emit the characteristic iron line, the redshift can be measured directly. The spectral and spatial data combined delineate the gravitational potential. The distribution of all matter, including dark matter, within distant clusters can be determined.

- A project of the European Space Agency **XMM** (renamed **XMM-Newton**), the X-ray Multi-Mirror Mission, is the second cornerstone of the Horizon 2000 program of the European Space Agency (ESA). XMM was launched on December 10, 1999. XMM provides images over a 30 arc minute field of view with moderate spectral resolution using the European Photon Imaging Camera (EPIC). High-resolution spectral information is provided by the Reflection Grating Spectrometer (RGS) that deflects half of the beam on two of the X-ray telescopes. The observatory also has a coaligned 30 cm optical/UV telescope called the Optical Monitor (OM). XMM observations include apart from clusters of galaxies the study of the cosmic X-ray background radiation, of normal and starburst galaxies, active galactic nuclei and quasars, stellar black holes, neutron stars, pulsars, binary stars, supernova remnants, the hot phase of the galactic ISM, cool gas, stellar coronae and comets.

  The XMM observations can be used to study several key properties of the hot intracluster medium. Spatially resolved spectroscopy will allow the determination of the radial variations of the gas density, temperature and metallicity. The knowledge of metallicities is important in the context of the chemical evolution of galaxies and gas in cluster.

X-ray observations can also be used to map the distribution of hot gas and thereby the distribution of matter in elliptical galaxies and clusters. Up to 30% of the total mass of galaxy clusters has been identified as X-ray emitting intracluster gas. This is a significant fraction of the formerly "missing" mass and XMM offers a possibility to trace even fainter emission than previous satellites (and thus more gas and thereby mass).

In some cases, e.g. the Perseus cluster, X-ray observations can also be used to study the interaction of a jet emanating from a radio core in a massive elliptical galaxy with the ambient hot gas.

Compared to the current generation of X-ray satellites, XMM offers improved capabilities in all three general observing techniques (imaging, spectroscopy and photometry), with the additional advantages of a wide energy passband and simultaneous optical/UV observations.

1.3 Important astrophysical production mechanisms

The main production mechanisms are shown on the Figure 1.4, particularly relevant are the *bremsstrahlung*, the *inverse Compton effect* and the *synchrotron radiation*.

Matter-antimatter annihilation (particularly e^+ e^- annihilation), radioactivity as well as energetic particles collisions are important processes for γ-rays production, which are for instance studied by the Integral satellite (and previously by the Compton Observatory).

In the following we will concentrate on the three main mechanisms we mentioned above, giving for each of them examples of astrophysical applications.

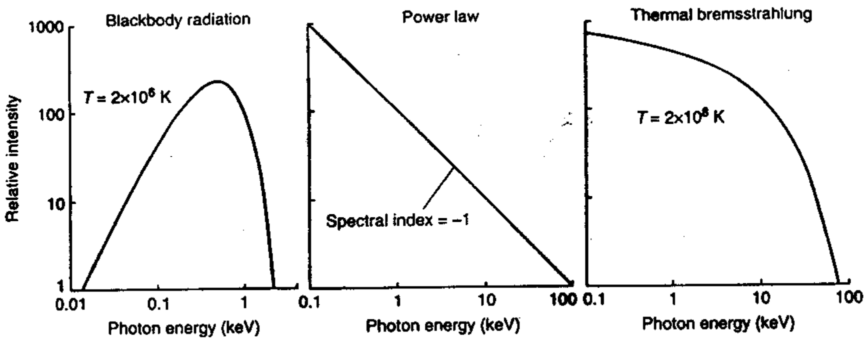

Figure 1.3: Three basic spectral forms expected from astrophysical processes. At the left is the blackbody spectrum expected from a dense object at a temperature of $2 \times 10^6\ K$. At the center is a power-law spectrum expected from *synchrotron radiation* produced in a region containing a magnetic field and high energy electrons. At the right is *thermal bremsstrahlung* from a thin, very hot gas. The different shapes are signatures of the physical production processes. From Ref. [8]

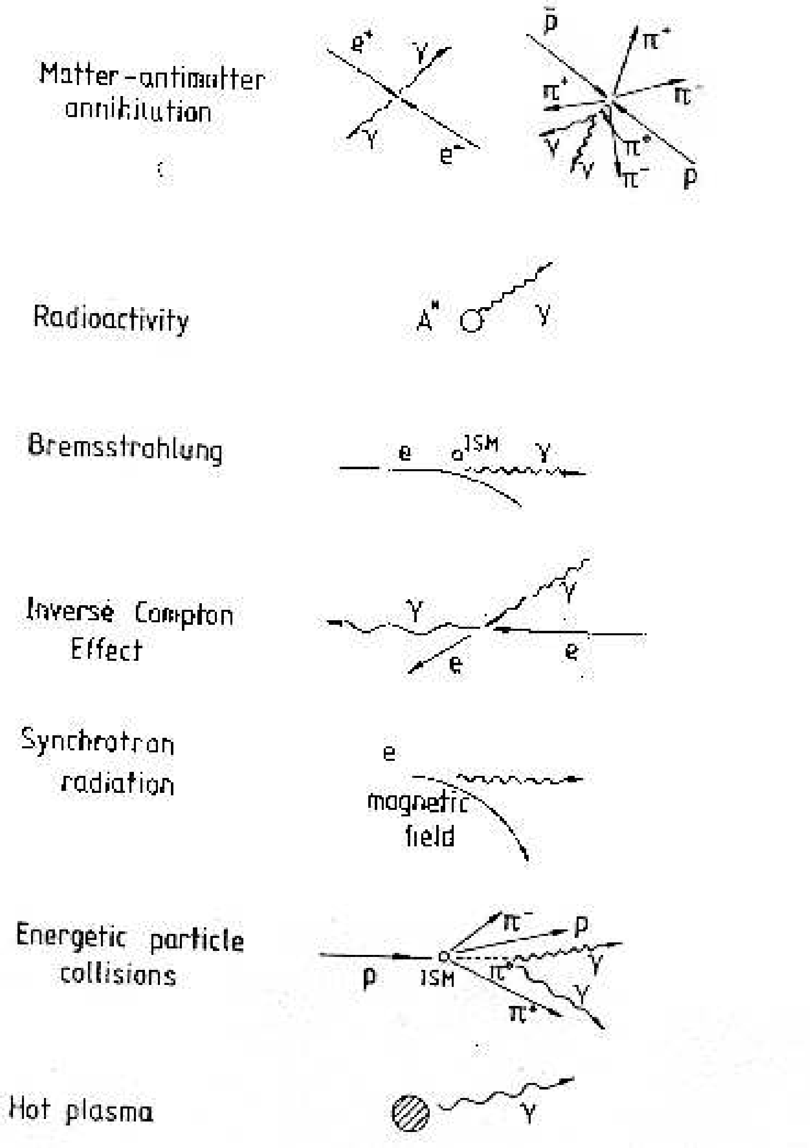

Figure 1.4: Summary of production mechanisms. A^* represents an excited nucleus. The other symbols have their usual meanings. From Ref. [9]

Chapter 2

Bremsstrahlung

Whenever a charged particle is accelerated or decelerated it emits electromagnetic radiation: *bremsstrahlung* is the radiation emitted in the encounter between an electron and a nucleus [10]. This process corresponds to that known as *free-free emission* in atomic physics, in the sense that the radiation corresponds to transitions between unbound states in the field of a nucleus. Whenever there is hot ionised gas in the Universe it emits *bremsstrahlung*.

From electrodynamics we know that the total radiation rate for an accelerated particle is given by Larmor's formula:

$$-\left(\frac{dE}{dt}\right)_{rad} = \frac{|\ddot{\vec{p}}_0\,|^2}{6\pi\;\epsilon_0\;c^3} = \frac{q^2\;|\ddot{\vec{r}}_0\,|^2}{6\pi\;\epsilon_0\;c^3}\;, \tag{2.1}$$

where $\vec{p}_0$ is the dipole momentum ($\vec{p}_0 = q\;\vec{r}_0$), q being the charge of the particle. In this formula the acceleration is the proper acceleration of the charged particle and the radiation loss is measured in the instantaneous rest frame of the particle.

We consider now the radiation loss of an accelerated charged particle moving at relativistic velocities. The radiation loss $\left(\frac{dE}{dt}\right)$ is a Lorentz invariant and is thus invariant under a Lorentz transformation. Consider the observer's reference frame $\mathcal{S}$ in which $\vec{a} = \ddot{\vec{r}}$ and $\vec{v} = \dot{\vec{r}}$. In the instantaneous rest frame of the particle, $\mathcal{S}\,'$, the acceleration four-vector is $(\vec{a}_0, 0)$, where $\vec{a}_0 = \ddot{\vec{r}}_0$ is the proper acceleration of the particle. The acceleration four-vector of a particle can be written as:

$$a^{\mu} = \gamma\left(\frac{d\gamma\vec{v}}{dt}, \frac{d\gamma}{dt}\right) = \left(\gamma^2\vec{a} + \left(\frac{\vec{v}\cdot\vec{a}}{c^2}\right)\gamma^4\vec{v}, \gamma^4\left(\frac{\vec{v}\cdot\vec{a}}{c^2}\right)\right)\;, \tag{2.2}$$

where $\gamma = \left(1 - \left(\frac{v}{c}\right)^2\right)^{-\frac{1}{2}}$ is the Lorentz factor. Accordingly, by equating the norms of the four-vectors in the reference frames $\mathcal{S}$ and $\mathcal{S}\,'$, one finds:

$$\vec{a}_0^2 = \gamma^4\left[\vec{a}^2 + \gamma^2\left(\frac{\vec{v}\cdot\vec{a}}{c}\right)^2\right]\;. \tag{2.3}$$

Since the radiation loss rate $\left(\frac{dE}{dt}\right)$ is a Lorentz invariant we have:

$$\left(\frac{dE}{dt}\right)_{\mathcal{S}} = \left(\frac{dE}{dt}\right)_{\mathcal{S}\,'} = \frac{q^2 \mid \vec{a}_0 \mid^2}{6\pi\ \epsilon_0\ c^3} = \frac{q^2 \mid \ddot{\vec{r}} \mid^2}{6\pi\ \epsilon_0\ c^3} \ ,$$

or using equation (2.3):

$$\left(\frac{dE}{dt}\right)_{\mathcal{S}} = \frac{q^2\ \gamma^4}{6\pi\ \epsilon_0\ c^3} \left[\vec{a}^2 + \gamma^2 \left(\frac{\vec{v}\cdot\vec{a}}{c}\right)^2\right] \ , \tag{2.4}$$

which is the relativistic generalisation[1]; notice that $\vec{a}$, γ and $\vec{v}$ are measured in the frame $\mathcal{S}$.

Usually $\vec{a}$ is written as the sum of a component parallel to the velocity $\vec{v}$, $\vec{a}_{\|}$, and a component perpendicular, $\vec{a}_{\perp}$: $\vec{a} = a_{\|} \cdot \vec{i}_{\|} + a_{\perp} \cdot \vec{i}_{\perp}$ (where $\vec{i}_{\|}$ and $\vec{i}_{\perp}$ are unitary vectors respectively parallel and orthogonal to the velocity vector $\vec{v}$) and $|\vec{a}|^2 = a_{\|}^2 + a_{\perp}^2$. Using this notation one finds:

$$\left(\frac{dE}{dt}\right)_{\mathcal{S}} = \frac{q^2\ \gamma^4}{6\pi\ \epsilon_0\ c^3} \left[a_{\perp}^2 + \gamma^2 a_{\|}^2\right] \ . \tag{2.5}$$

Consider now the spectral distribution of the radiation of an accelerated electron ($q = e$), in particular the Fourier transform of the acceleration:

$$\begin{aligned} \dot{\vec{v}}\,(t) &= \tfrac{1}{\sqrt{2\pi}} \int\limits_{-\infty}^{+\infty} \dot{\vec{v}}\,(\omega)\, e^{-i\omega t} d\omega \\ \dot{\vec{v}}\,(\omega) &= \tfrac{1}{\sqrt{2\pi}} \int\limits_{-\infty}^{+\infty} \dot{\vec{v}}\,(t)\, e^{+i\omega t} dt \ . \end{aligned} \tag{2.6}$$

Parseval's theorem states then:

$$\int\limits_{-\infty}^{+\infty} |\dot{\vec{v}}\,(\omega)\,|^2 d\omega = \int\limits_{-\infty}^{+\infty} |\dot{\vec{v}}\,(t)\,|^2 dt \ . \tag{2.7}$$

Accordingly ($\ddot{\vec{r}} = \dot{\vec{v}}$) we get for the integrated radiation loss:

$$\begin{aligned} \int\limits_{-\infty}^{+\infty} \frac{dE}{dt} dt = \int\limits_{-\infty}^{+\infty} \frac{e^2}{6\pi\ \epsilon_0\ c^3} |\dot{\vec{v}}(t)|^2 dt = \\ \int\limits_{-\infty}^{+\infty} \frac{e^2}{6\pi\ \epsilon_0\ c^3} |\dot{\vec{v}}(\omega)|^2 d\omega = 2 \int\limits_{0}^{\infty} \frac{e^2}{6\pi\ \epsilon_0\ c^3} |\dot{\vec{v}}(\omega)|^2 d\omega \ . \end{aligned} \tag{2.8}$$

[1]For $\frac{v}{c} \ll 1,\ \gamma \to 1$ and equation (2.4) reduces to equation (2.1).

As the total emitted radiation is defined as $\int_0^\infty I(\omega)d\omega$, we find:

$$I(\omega) = \frac{e^2}{3\pi\ \epsilon_0\ c^3}|\dot{\vec{v}}(\omega)|^2 = \frac{e^2}{3\pi\ \epsilon_0\ c^3}\left[a(\omega)_\parallel^2 + a(\omega)_\perp^2\right] \ . \tag{2.9}$$

The acceleration of an electron, due to an electrostatic field of a (high energy) proton or nucleus, can be split into its components parallel and perpendicular to the particle's trajectory; supposing that the x-axis and the z-axis are respectively parallel and perpendicular to the trajectory, one finds the following expressions:

$$\begin{aligned} a_\parallel &= \dot{v}_x = -\tfrac{eE_x}{m_e} = \tfrac{\gamma Z e^2 vt}{4\pi\ \epsilon_0\ m_e(b^2+(\gamma vt)^2)^{\frac{3}{2}}} \\ a_\perp &= \dot{v}_z = -\tfrac{eE_z}{m_e} = \tfrac{\gamma Z e^2 b}{4\pi\ \epsilon_0\ m_e(b^2+(\gamma vt)^2)^{\frac{3}{2}}} \ , \end{aligned} \tag{2.10}$$

where Ze is the charge of the nucleus and b is the distance of closest approach of the electron to the nucleus (at $t = 0$). It is assumed that the electron is initially at rest and that the electron is not accelerated to relativistic energies. Thus the magnetic field can be neglected.

Now we have to compute the Fourier transform of the acceleration as given in equation (2.10):

$$\begin{aligned} a_\parallel(\omega) &= \frac{1}{\sqrt{2\pi}}\int_{-\infty}^{+\infty}\frac{\gamma Z e^2 vt}{4\pi\ \epsilon_0\ m_e\ (b^2+(\gamma vt)^2)^{\frac{3}{2}}}e^{+i\omega t}dt \\ &= \frac{1}{\sqrt{2\pi}}\frac{Ze^2}{4\pi\ \epsilon_0\ m_e}\frac{1}{\gamma bv}\int_{-\infty}^{+\infty}\frac{x}{(1+x^2)^{\frac{3}{2}}}e^{\left(i\frac{\omega b}{\gamma v}\right)}dx \\ &= \frac{1}{\sqrt{2\pi}}\frac{Ze^2}{4\pi\ \epsilon_0\ m_e}\frac{1}{\gamma bv}I_1(y) \end{aligned} \tag{2.11}$$

with $x = \frac{\gamma vt}{b}$, $y = \frac{\omega b}{\gamma v}$ and $I_1(y) = 2iyK_0(y)$, where $K_0(y)$ is a modified Bessel function of order 0.

Analogously

$$a_\perp(\omega) = \frac{1}{\sqrt{2\pi}}\frac{Ze^2}{4\pi\ \epsilon_0\ m_e}\frac{1}{bv}I_2(y) \ , \tag{2.12}$$

where $I_2(y) = 2yK_1(y)$, with $K_1(y)$ being a modified Bessel function of order 1.

Accordingly we find for the radiation spectrum of an electron in the encounter with the charged nucleus (equation (2.9)):

$$I(\omega) = \frac{Z^2 e^6}{24\pi^4\epsilon_0{}^3\ c^3\ m_e{}^2}\ \frac{\omega^2}{\gamma^2 v^2}\left[\frac{1}{\gamma^2}\ K_0^2\left(\frac{\omega b}{\gamma v}\right) +\ K_1^2\left(\frac{\omega b}{\gamma v}\right)\right] . \tag{2.13}$$

For $y \ll 1$, $K_0(y) = -ln(y)$ and $K_1(y) = \frac{1}{y}$; instead for $y \gg 1$, $K_0(y) = K_1(y) = \sqrt{\frac{\pi}{2y}}\ e^{-y}$.

Thus at high frequencies we find an exponential cut-off in the radiation spectrum.

In the low frequency limit the spectrum has the form

$$I(\omega) = \frac{Z^2 e^6}{24\pi^4 \epsilon_0{}^3\, c^3\, m_e{}^2} \frac{1}{b^2 v^2} \left[1 - \frac{1}{\gamma^2} \left(\frac{\omega b}{\gamma v} \right)^2 ln^2 \left(\frac{\omega b}{\gamma v} \right) \right] . \tag{2.14}$$

In this limit the second term in the square brackets can be neglected and hence $I(\omega)$ is constant [2].

In the high frequency limit the spectrum reduces to the following:

$$I(\omega) = \frac{Z^2 e^6}{48\pi^3 \epsilon_0{}^3 c^3 m_e{}^2} \frac{1}{\gamma v^3} \left[\frac{1}{\gamma^2} + 1 \right] e^{-\frac{2\omega b}{\gamma v}} . \tag{2.15}$$

The duration of the relativistic collision is $\tau \simeq \frac{2b}{\gamma v}$, which corresponds to a frequency $\nu \sim \frac{1}{\tau}$ or $\omega \simeq \frac{\pi v \gamma}{b}$. The exponential cut-off means that little power is emitted at frequencies greater than $\omega \simeq \frac{\gamma v}{b}$.

Let's consider in the following the low frequency limit, where, moreover, the second term in the square brackets can be neglected, so that $I(\omega) = const$. As next we have to integrate over all relevant collision parameters which contribute to the radiation at frequency ω. If the electron is moving relativistically, the number density of nuclei it observes is enhanced by a factor γ, due to the relativistic length contraction. Therefore, in the moving frame of the electron, $N' = \gamma N$, where N is the space density of nuclei in the laboratory frame. The number of encounters per second is, accordingly, $N'v$.

Thus we get for the radiation spectrum in the frame of the electron:

$$\begin{aligned} I(\omega) &= \frac{Z^2 e^6}{24\pi^4\, \epsilon_0{}^3\, c^3\, m_e{}^2} \int_{b_{min}}^{b_{max}} \frac{1}{b^2 v^2} 2\pi b \gamma N v db \\ &= \frac{Z^2 e^6 N \gamma}{12\pi^3\, \epsilon_0{}^3\, c^3\, m_e{}^2} \frac{1}{v} ln \left(\frac{b_{max}}{b_{min}} \right) . \end{aligned} \tag{2.16}$$

2.1 Non-relativistic and thermal bremsstrahlung

We consider two cases:

i. we evaluate the total energy loss rate by *bremsstrahlung* for high energetic but still non-relativistic electrons;

ii. we compute the continuum spectrum and radiation loss rate of an hot ionised gas in which the velocity distribution of the electrons at temperature T is Maxwellian.

[2] $\omega \rightarrow 0$ means a very short period, thus the momentum impulse is just a δ function, whose Fourier transform is a constant.

In both cases we neglect the relativistic correction factors ($\gamma \rightarrow 1$).

We have then to insert into equation (2.16) the correct expression for b_{max} and b_{min}. We should only integrate on those values of b for which $\frac{\omega b}{v} \approx 1$, since for larger values of b the radiation at frequency ω lies on the exponential tail of the spectrum and thus gives negligible contribution. Thus, $b_{max} = \frac{v}{\omega}$. For b_{min} we consider two possibilities. For small velocities, $v < \left(\frac{Z}{137}\right) c$, one can use the classical limit given by[3] $b_{min} = \frac{Ze^2}{8\pi\ \epsilon_0\ m_e\ v^2}$. This is appropriate when considering the *bremsstrahlung* of a region of ionised hydrogen at $T \simeq 10^4 K$. At higher temperatures and thus higher velocities ($v \geq \left(\frac{Z}{137}\right) c$) one has to consider the quantum mechanical constraints, then $b_{min} \simeq \frac{\hbar}{2m_e v}$, which is obtained by simply considering the Heisenberg uncertainty principle.

This way we get for the radiation spectrum

$$I(\omega) = \frac{Z^2 e^6 N}{12\pi^3 {\epsilon_0}^3 c^3 {m_e}^2}\ \frac{1}{v}\ ln\Lambda\ , \tag{2.17}$$

where $\Lambda = \frac{8\pi\epsilon_0 m_e v^3}{Ze^2\omega}$ for low velocities, and $\Lambda = \frac{2m_e v^2}{\hbar\omega}$ for high velocities. To get the total energy loss rate of an high energy particle one has to integrate equation (2.17) over all frequencies. This means integrating from 0 to ω_{max}, where ω_{max} corresponds to the cut-off $b_{min} \simeq \frac{\hbar}{2m_e v}$ for high velocities. The maximum amount of energy which can be emitted in a single encounter is $\hbar\omega \simeq \frac{1}{2} m_e v^2$, as it corresponds to the kinetic energy of the electron. Accordingly $\omega_{max} \approx \frac{m_e v^2}{2\hbar}$ and we get:

$$\begin{aligned} -\left(\frac{dE}{dt}\right)_{brems} &\simeq \int_0^{\omega_{max}} \frac{Z^2 e^6 N}{12\pi^3\ {\epsilon_0}^3\ c^3\ {m_e}^2}\ \frac{1}{v}\ ln\Lambda\ d\omega \\ &\simeq \frac{Z^2 e^6 N v}{24\pi^3\ {\epsilon_0}^3\ c^3\ m_e\ \hbar}\ ln\Lambda \simeq const\ Z^2\ Nv\ , \end{aligned} \tag{2.18}$$

where the ω dependence in $ln\Lambda$ has been neglected. Since v is proportional to the square root of the kinetic energy E, we have that $-\frac{dE}{dt}$ is proportional to $E^{\frac{1}{2}}$.

As next we compute the *bremsstrahlung* of a gas at temperature T, with the electron velocity distributed according to a Maxwellian as follows:

$$n_e(v) = 4\pi\ N_e\ \left(\frac{m_e}{2\pi\ kT}\right)^{\frac{3}{2}}\ v^2\ e^{-\frac{m_e\ v^2}{2kT}}\ , \tag{2.19}$$

where N_e is the electron density, which can be a function of the spatial position.

The spectral emissivity of the plasma, defined as the emitted energy per unit time, frequency and volume, is given as

$$k_\nu = \int_0^\infty n_e(v)\ I(\omega, v)\ dv \qquad (\omega = 2\pi\nu)\ , \tag{2.20}$$

[3]The closest distance of approach corresponds to that collision parameter at which the electrostatic potential energy of interaction of the high energy particle and the electron is equal to the maximum possible energy transfer.

where $I(\omega, v)$ is given by equation (2.17). One gets as follows:

$$k_\nu = \frac{1}{3\pi^2} \left(\frac{\pi}{6}\right)^{\frac{1}{2}} \frac{Z^2 \, e^6}{\epsilon_0^3 \, c^3 \, m_e^2} \left(\frac{m_e}{kT}\right)^{\frac{1}{2}} g(\nu, T) \, N \, N_e \, e^{-\frac{h\nu}{kT}}$$
$$= 6.8 \times 10^{-51} \, Z^2 \, T^{\frac{1}{2}} \, N \, N_e \, g(\nu, T) \, e^{-\frac{h\nu}{kT}} \qquad [\, W \, m^{-3} \, Hz^{-1} \,] \,, \quad (2.21)$$

where N is the density of the nuclei (for instance protons) and N_e the electron density, $g(\nu, T)$ is the so called *Gaunt factor*, which is the proper form of the term in Λ integrated over the velocity. In terms of quantum mechanics the *Gaunt factor* gives the number of states.

According to the frequency interval considered the *Gaunt factor* can be approximated, such that suitable forms for the radio and the X-ray wavelengths are respectively:

$$g(\nu, T) = \frac{\sqrt{3}}{2\pi} \left[ln \left(\frac{128 \, \epsilon_0^2 \, kT^3}{m_e \, e^4 \, \nu^2 \, Z^2} \right) - \tilde{\gamma}^{\frac{1}{2}} \right]$$

in the radio range[4], and

$$g(\nu, T) = \frac{\sqrt{3}}{\pi} \, ln \left(\frac{kT}{h\nu} \right)$$

in the X-ray range.

By integrating the spectral emissivity k_ν over the frequency ν one finds the total energy loss rate of the plasma:

$$- \left(\frac{dE}{dt} \right)_{brems} = 1.435 \times 10^{-40} \, Z^2 \, T^{\frac{1}{2}} \, \bar{g} \, N \, N_e \quad [\, W \, m^{-3} \,] \,, \qquad (2.22)$$

where $\bar{g}$ is the averaged *Gaunt factor* over frequency, which turns out to be in the range $1.1 - 1.5$, so that we will in the following assume $\bar{g} = 1.2$.

2.2 Bremsstrahlung loss of a galaxy cluster

Galaxies are not strewn randomly throughout the universe. Instead, nearly all galaxies are found in associations, either in groups or in clusters. Groups generally have less than 50 members and are about $1.4 h_{50}^{-1} Mpc$ across[5]. On the other hand, the clusters may contain from approximately 50 to thousands of galaxies, within a region of space about $6 h_{50}^{-1} Mpc$. Groups of galaxies, clusters of galaxies and clusters of clusters (called superclusters) make up the large scale structure of the universe [13].

The Virgo cluster of galaxies was first recognised in the eighteenth century, located where the constellations of Virgo and Coma Berenices meet. The center is located about 16 Mpc from Earth. This rich, irregular cluster is a collection

[4] $\tilde{\gamma} = 0.577...$ is the Euler constant.

[5] The Hubble constant is parametrized as $H_0 = 50 h_{50}$ km/(sec Mpc).

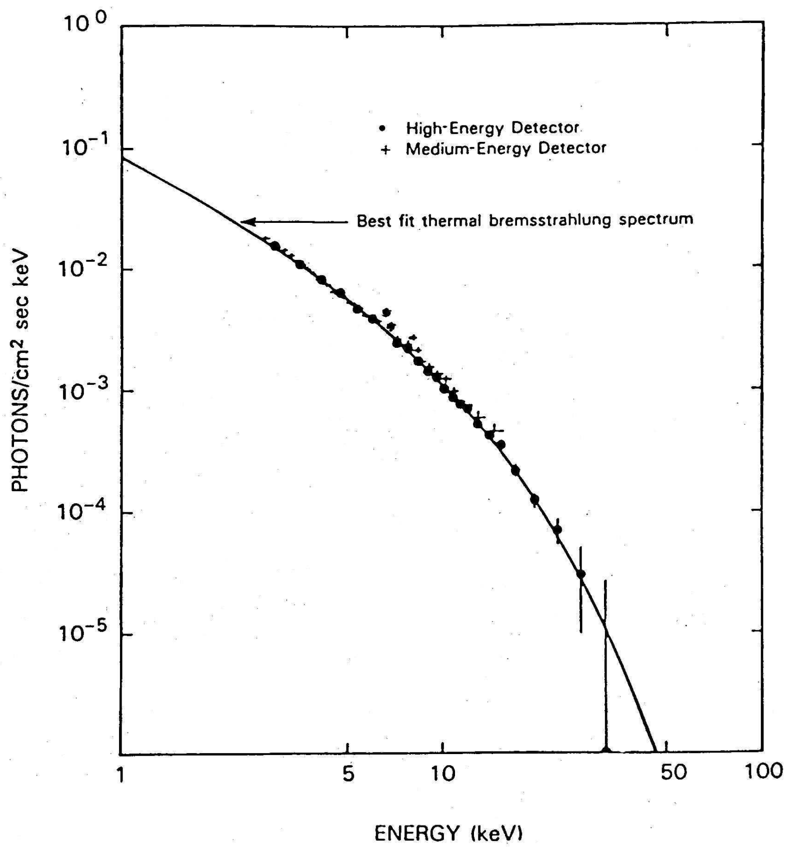

Figure 2.1: HEAO-1 A-2 low resolution X-ray spectra of clusters, showing the Fe K line at about $7keV$. The plot gives the number flux of X-ray photons per $cm^2\ sec\ keV$ versus photon energy in keV, for the Coma cluster. From Ref. [11]

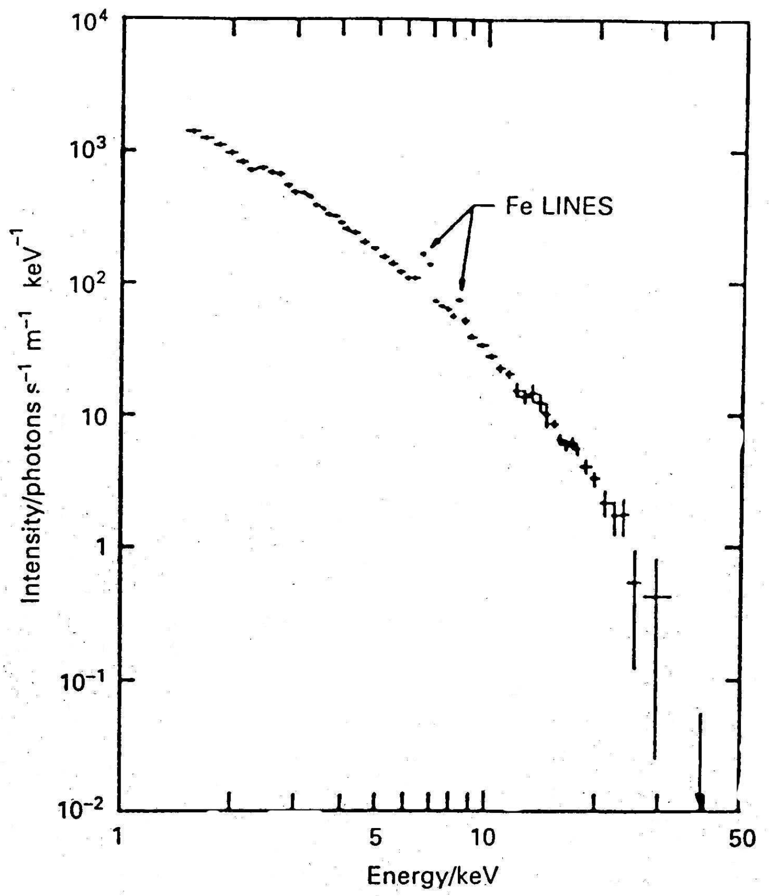

Figure 2.2: The X-ray spectrum of the Perseus cluster of galaxies observed by the HEAO-A2 instrument. The continuum emission can be accounted for by the thermal bremsstrahlung of hot intracluster gas at a temperature corresponding to $kT = 6.5\ keV$, i.e. $T = 7.5 \times 10^7\ K$. The thermal nature of the radiation is confirmed by the observation of the Lyα and Lyβ emission lines of highly ionised iron, Fe^{+25}, at energies of 6.7 and 7.9 keV respectively. The ionisation potential of Fe^{+24} is 8.825 keV and hence the gas must be very hot. From Ref. [12]

of approximately 250 large galaxies and more than 2000 smaller ones, contained within a region about 3 Mpc across. Like most irregular clusters, the Virgo cluster is made up of all types of galaxies and the center is dominated by three of the cluster's four giant elliptical galaxies (M84, M86 and M87).

The nearest rich, regular cluster of galaxies is the Coma cluster. It is believed that the Coma cluster consists of perhaps 10000 galaxies, most of them dwarf elliptical that are too faint to be seen. It contains 1000 bright galaxies, but only 15 per cent of them are spirals and irregulars. At the cluster's center there are two large, luminous cD elliptical.

In 1966, X-ray emission was detected from the region around the galaxy M87 in the center of the Virgo cluster. In fact, M87 was the first object outside of our galaxy to be identified as a source of astronomical X-ray emission. Five years later, X-ray sources were also detected in the directions of the Coma and Perseus clusters. Since these are three of the nearest rich clusters, it was suggested that clusters of galaxies might generally be X-ray sources. The launch of the UHURU X-ray astronomy satellite permitted a survey of the entire sky for X-ray emission [14] and established that this was indeed the case. These early UHURU observations indicated that many clusters were bright X-ray sources with luminosities typically in the range of 10^{43-45} ergs/sec. The X-ray sources associated with clusters were found to be spatially extended; their sizes were comparable to the size of the galaxy distribution in the cluster. Unlike other bright X-ray sources but consistent with their spatial extends, cluster X-ray sources did not vary temporally in their brightness.

When cluster of galaxies were found to be an important class of X-ray sources, there were a number of suggestions as to the primary X-ray emission mechanism. The three most prominent ideas were that the emission resulted from thermal bremsstrahlung from a hot diffuse intracluster gas [15] or that the emission resulted from inverse Compton scattering of cosmic background photons up to X-ray energies by relativistic electrons within the cluster [16, 17], or that the emission was due to a population of individual stellar X-ray sources, like those found in our galaxy [18].
Models in which the emission comes from diffuse thermal gas predict:

- The spectrum will be roughly exponential, the intensity (in $ergs$ per cm^2 per $second$ per $Hertz$) varies as $I_\nu \sim \exp(-h\nu/\kappa_B T_g)$, where T_g is the gas temperature.

- The thermal velocity of protons in the gas $\sim (\kappa_B T_g/m_p)^{1/2}$ will be comparable to the velocity of the galaxies in the cluster, as both are bound by the same gravitational potential.

- There will be no strong low-energy photoabsorption.

- Emission lines will be present if the gas contains significant contamination of heavy elements like iron.

Observations have provided a great deal of support for the thermal bremsstrahlung model, and have generally not supported the other two suggestions.

Thus the observed X-ray emission from the cluster must be thermal bremsstrahlung from a hot plasma. The interpretation requires that the space between galaxies in clusters be filled with very hot ($\backsim 10^8 K$), low density ($\backsim 10^{-3} atoms/cm^{-3}$) plasma.

The following heating mechanisms have been proposed in order to explain such a large gas temperature [13]:

- If the gas is initially cold and located at large distance from the cluster and subsequently falls into the cluster, its kinetic energy will be converted to thermal energy due to friction and multiple scattering. The infalling gas can be heated up to temperatures:

$$T_g \approx 5 \times 10^8 \left(\frac{\sigma_r}{10^3 km/s} \right)^2 K,$$

  where σ_r is the line-of-sight velocity dispersion of the cluster. This temperature is a factor 5-10 times larger than the observed X-ray temperature. This discrepancy can be explained as following: the gas was initially bound in the cluster (thus the temperature is overestimated) or the gas fell in at the same time the cluster collapsed (the heating is then caused by rapid variation of the gravitational potential during violent relaxation). These models cannot explain the observed iron abundances, thus another mechanism may be responsible.

- Ejection from galaxies which move through the intracluster gas or supernova explosions could heat up the gas and they may be important for the enrichment of the intracluster gas.

- The heating may be due to friction between the gas and the galaxies that are constantly moving throughout the cluster.

- The relativistic electrons responsible for radio emission in clusters can interact with the gas and may heat it. But models with relativistic electrons suffer from these general problems: the total energy requirements are extreme for a single radio source, the radio sources generally occupy only a small fraction of the cluster. Furthermore it is difficult to explain how several discrete sources would heat the whole gas.

The X-ray emission from clusters is due to diffuse intraclusters gas at a temperature of $T_{gas} \simeq 10^8\ K$ and an atomic density of $n \simeq 10^{-3}\ cm^{-3}$. At such temperatures and densities, the primary emission process for a gas composed mainly of hydrogen is the *thermal bremsstrahlung* emission. If the intraclusters gas is mainly at a single temperature, then equation (2.21) indicates that the X-ray spectrum should be close to an exponential function of the frequency. Indeed, the observed X-ray spectra of clusters of galaxies are generally fairly well fitted by equation (2.21), with gas temperatures from 2×10^7 to $10^8\ K$.

The clearest evidence in favour of the *thermal bremsstrahlung model* is the detection of strong X-ray line emission from clusters, in particular the strong $\sim 7\ keV\ Fe$ line.

Consider a cluster of galaxies with typical density $n \simeq 10^{-3}\ cm^{-3}$ (corresponding to $N \sim 10^3\ m^{-3}$), mainly protons, and a similar density of electrons (charge neutrality). Assuming spherical symmetry for the cluster and a typical radius of $\simeq 0.5\ Mpc$ with $Z = 1$, $T \simeq 10^7\ K$, $\bar{g} = 1.2$, one finds the following expression for the total X-ray luminosity:

$$L = \int -\left(\frac{dE}{dt}\right)\, dV \cong 8 \times 10^{43}\ erg\ s^{-1} \quad (8 \times 10^{36}\ W)\,, \tag{2.23}$$

where $-\left(\frac{dE}{dt}\right)$ is given by equation (2.22).

Typically one finds X-ray luminosities for clusters in the range $10^{43} - 10^{45}\ erg\ s^{-1}$. Usually one observes a flux of photons coming from the cluster at a given frequency; with $\mathcal{L}_\nu = \int k_\nu\, dV$, the observed flux is given by $\frac{\mathcal{L}_\nu}{4\pi D^2}$, where D is the distance from the cluster, and thus its frequency dependence scales as $g(\nu, T) e^{-\frac{h\nu}{kT}}$, with $g(\nu, T) \sim ln\left(\frac{kT}{h\nu}\right)$ in the X-ray range.

The X-ray continuum emission from an hot diffuse plasma is due primarily to three processes: *thermal bremsstrahlung* (*free-free emission*), recombination (*free-bound emission*) and two-photon decay of metastable levels. At the high temperatures which predominate in clusters of galaxies *thermal bremsstrahlung* is the main X-ray emission process. For solar abundances, the emission is mainly due to hydrogen and helium.

Since the intracluster gas contains also *heavy* elements (typically corresponding to values from 0.3 to 0.5 times solar metallicity) there is also line emission (for instance from Iron and Oxygen).

Processes contributing to X-ray line emission from a diffuse plasma include collisional excitation of valence or inner shell electrons, radiative and dielectronic recombination, inner shell collisional ionization and radiative cascades following any of these processes.

The emissivity due to a collisionally excited line is usually written as:

$$\int k_\nu^{line}\, d\nu = N(x^i)\, N_e\, \frac{h^3\, \nu\, \Omega\, (T_g)\, \mathcal{B}}{4\, \omega_{gs}(x^i)} \left[\frac{2}{\pi^3\, m_e^3\, kT_g}\right] e^{-\frac{\Delta E}{kT_g}}\ , \tag{2.24}$$

where x^i is the ion of the species i, ω_{gs} is the statistical weight of the ground state, $h\nu$ is the energy of the transition, ΔE is the excitation energy above the ground state of the excited level, $\mathcal{B}$ is the branching ratio for the line[6] and Ω is the *collision strength*, which depends on the gas temperature T_g.

[6]The probability that the upper state decays through this transition.

Nowadays there are very efficient compilations of the emissivities for X-ray lines and continua, which are used to analyse the data of satellites like **XMM-Newton** and **CHANDRA**.

As next we give a crude estimate for the cooling time of the intergalactic gas.

The internal energy of the electron gas is $E \simeq \frac{3}{2}\, N_e kT$, and on the other hand the radiation energy loss rate is given by equation (2.22) (setting $Z = 1$ and $N \simeq N_e$). This way the cooling time t_{cool} is proportional to $E/\dot{E}$, namely

$$t_{cool} \propto \frac{E}{\dot{E}} = \frac{\frac{3}{2}\, N_e\, kT}{1.43 \times 10^{-40}\, T^{\frac{1}{2}}\, N_e^2}$$
$$= 4.6 \times 10^{10} \left(\frac{N_e}{10^3\ m^{-3}}\right)^{-1} \left(\frac{T}{10^8\ K}\right)^{\frac{1}{2}}\ years. \tag{2.25}$$

We thus see that the cooling time for the intracluster plasma is comparable, if not even higher, to the age of the Universe, which is about $15 \times 10^9\ years$.

2.3 Determination of the total mass of a cluster of galaxies

We assume that the gas is in hydrostatical equilibrium such that the following equation holds:

$$\nabla P = -\rho_{gas}\, \nabla\Phi(r)\ , \tag{2.26}$$

where P is the pressure, which is given[7] by:

$$P = \rho_{gas}\, \frac{kT_g}{\mu\, m_p}\ , \tag{2.27}$$

where μ is the average atomic weight ($\simeq 0.63$), m_p the proton mass and $\Phi(r)$ is the gravitational potential[8] of the cluster.

Then one obtains from equation (2.26):

$$\frac{1}{\rho_{gas}}\frac{dP}{dr} = -\frac{d\Phi(r)}{dr} = -\frac{G\, M(r)}{r^2} \qquad \rho_{gas} = (m_e + m_p)N_e\ , \tag{2.28}$$

and thus for the total gravitating mass $M(r)$ inside the radius r:

$$M(r) = -\frac{kT_g(r)\, r}{\mu\, m_p\, G}\left(\frac{d\, ln(\rho_g(r))}{d\, ln(r)} + \frac{d\, ln(T_g(r))}{d\, ln(r)}\right)\ , \tag{2.29}$$

where $\rho_g(r)$ and $T_g(r)$ are respectively the gas density profile and the temperature profile.

In principle $\rho_g(r)$ and $T_g(r)$ can be measured with X-ray satellites (provided the spatial and spectral resolution are high enough). However, one observes the

[7]Assuming an ideal gas.

[8]Assumed spherically symmetric.

bi-dimensional projected surface brightness, from which one has to reconstruct the three-dimensional profiles. This can be done when assuming spherical symmetry.

Often one assumes an isothermal gas, so that the temperature is constant, $T_g = const$, and is given by the *bremsstrahlung* continuum. For the gas density one makes the following Ansatz (β-model) [19]:

$$\rho_g(r) = \rho_0 \left(1 + \left(\frac{r}{r_c}\right)^2\right)^{-\frac{3}{2}\beta} , \tag{2.30}$$

where r_c is the core radius, ρ_0 is the central density and β is a free parameter. Using equation (2.30), equation (2.29), for an isothermal gas, turns into:

$$\begin{aligned} M(r) &= \frac{3\beta}{G} \frac{kT_g\, r}{\mu\, m_p} \frac{\left(\frac{r}{r_c}\right)^2}{1 + \left(\frac{r}{r_c}\right)^2} \\ &= 1.13 \times 10^{15}\, \beta\, \frac{T_g}{10\, keV} \frac{r}{Mpc} \frac{\left(\frac{r}{r_c}\right)^2}{1 + \left(\frac{r}{r_c}\right)^2} M_\odot , \end{aligned} \tag{2.31}$$

where we assumed $\mu = 0.59$.

For an isothermal gas which follows a β-model, one finds for the X-ray surface brightness (bi-dimensional projection):

$$S_x(\theta) = S_0 \left(1 + \left(\frac{\theta}{\theta_c}\right)^2\right)^{-3\beta+\frac{1}{2}} , \tag{2.32}$$

where θ is the angle under which an observer sees the bi-dimensional projected distance r (accordingly θ_c for r_c).

Typical values for β are in the range $0.65 - 0.9$. For the Coma cluster one finds that the gas contributes about 30% to the total mass.

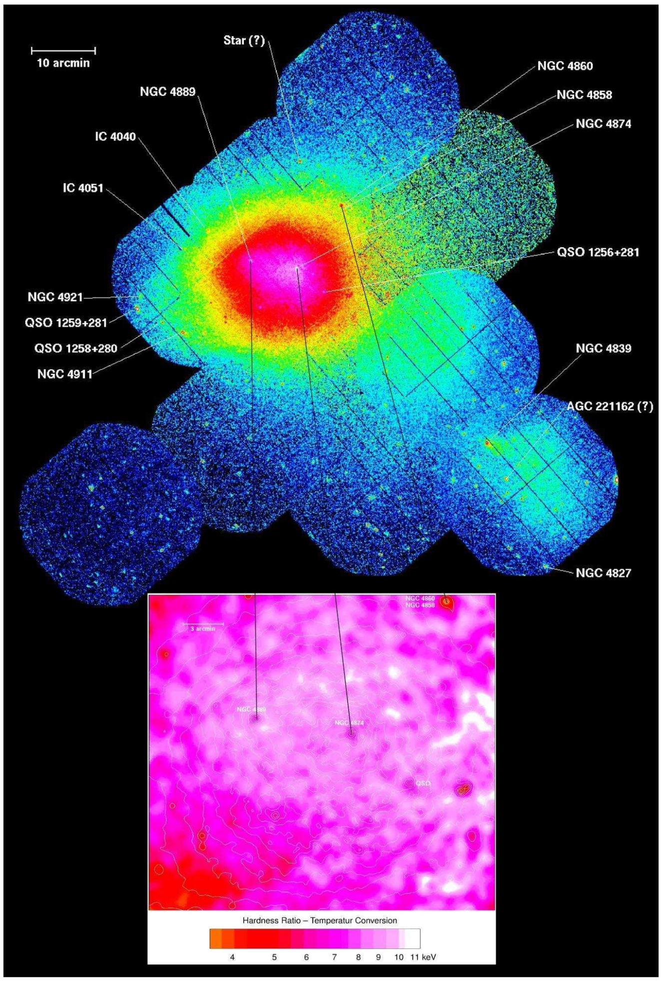

6 December 2000

Figure 2.3: The Coma Cluster, an aggregate thousands of galaxies, as observed by XMM-Newton. The picture is a mosaic of 12 partially overlapping pointings obtained with the EPIC-pn camera. The cluster was chosen during XMM-Newton's performance verification phase to prove the observatory's ability to map and analyse data from large extended X-ray sources.
Bottom, a close-up view of the temperature structure in the inner region of the Coma Cluster of galaxies, highlighting the X-ray hardness and corresponding temperatures around the giant elliptical galaxies NGC 4889 and NGC 4874 and the gas in the central part of the cluster. Courtesy U. Briel, Max-Planck Institut für extraterrestrische Physik, Garching, Germany.

Chapter 3

Photoelectric absorption

For low photon energies, $\hbar\omega \ll m_e\, c^2$, the dominant process by which photons lose energy is photoelectric absorption.

If the energy of the incident photon is $\hbar\omega$, it can eject electrons which have binding energy $E_I \leq \hbar\omega$ from atoms, ions or molecules. The remaining energy $(\hbar\omega - E_I)$ goes into the kinetic energy of the ejected electron[1].

The energy levels of the atoms for which $\hbar\omega = E_I$ are called *absorption edges*, because ejection of electrons from these energy levels is not possible if the photons are at lower energy. For photons with higher energy, the cross-section for photoelectric absorption from this level decreases roughly as ν^{-3}.

The absorption cross-section for photons with energy $\hbar\omega \gg E_I$, but $\hbar\omega \ll m_e\, c^2$, due to the ejection of electrons from the K-shell[2] of atoms, can be computed in quantum mechanics and is as follows:

$$\sigma_K = 4\sqrt{2}\,\sigma_T\,\alpha^4\,Z^5\,\left(\frac{m_e\,c^2}{\hbar\omega}\right)^{\frac{7}{2}}\,, \tag{3.1}$$

where $\alpha = \frac{e^2}{4\pi\,\epsilon_0\,\hbar c}$ is the fine structure constant, and $\sigma_T = \frac{e^4}{6\pi\,{\epsilon_0}^2\,m_e^2\,c^4}$ is the Thomson cross-section. Since $\sigma_K \sim Z^5$ there is a strong dependence on the atomic number, and thus heavy elements, although less abundant than hydrogen, contribute substantially to the absorption cross-section.

An important application of the photoelectric absorption is the hard ultraviolet and X-ray absorption due to interstellar matter.

A useful formula for the X-ray absorption is given by the optical depth $\tau_x = \int \sigma_x N_H\,dl$, where σ_x is the absorption cross-section and N_H is the number density of hydrogen atoms, thus $\int N_H\,dl$ corresponds to the column density. One finds:

$$\tau_x = 2\times 10^{-26}\,\left(\frac{\hbar\omega}{1keV}\right)^{-\frac{8}{3}}\,\int N_H\,dl\,. \tag{3.2}$$

[1]Photoelectric effect by Einstein 1905

[2]i.e. from the 1s level.

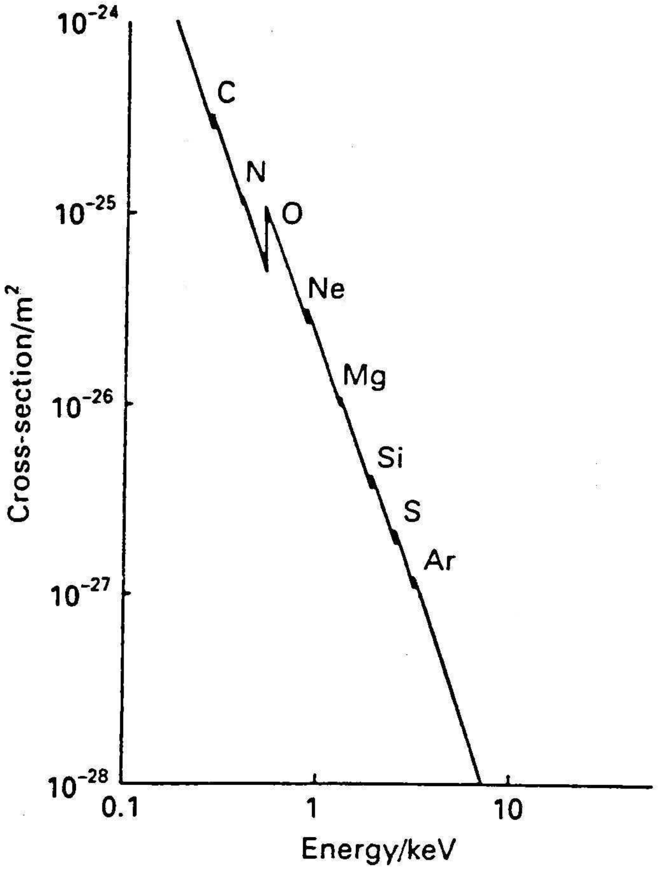

Figure 3.1: The absorption cross-section for interstellar gas with typical cosmic abundances of the chemical elements. The discontinuities in the absorption cross-section as a function of energy are associated with the K-shell absorption edges of the elements indicated. The optical depth of the medium is given by $\tau = \int \sigma_x \, (E) \; N_H \; dl$ where N_H is the number density of hydrogen atoms. From Ref. [20]

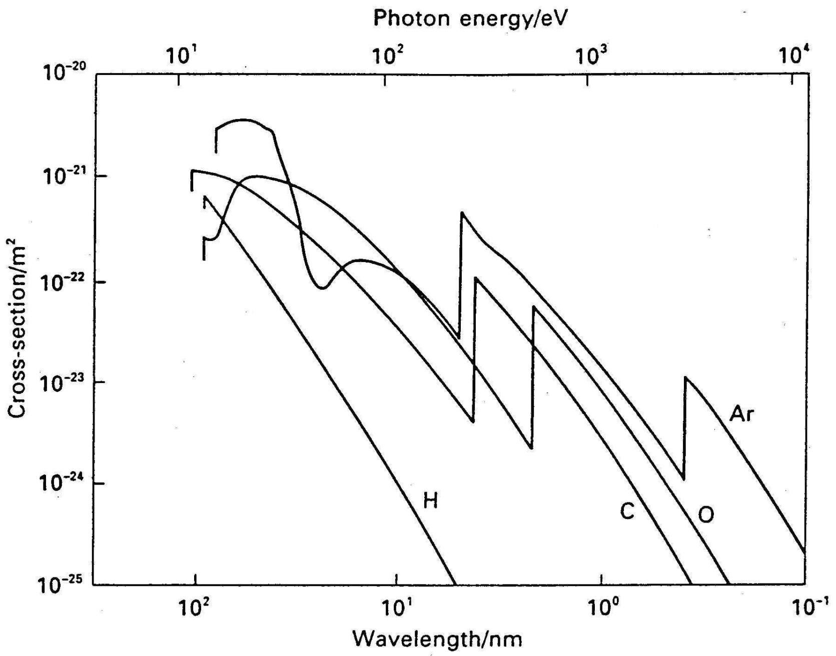

Figure 3.2: The absorption coefficients for hydrogen, carbon, oxygen and argon atoms as a function of photon energy (or wavelength). From Ref. [21]

For $\hbar\omega \gtrsim 1keV$ the photoelectric absorption is generally no longer relevant. Indeed, typical column densities are of the order 10^{25-26} H atoms per square meter (for instance towards the Magellanic clouds), then for $\hbar\omega \sim 1keV \quad \tau_x \sim \left(\frac{1keV}{\hbar\omega}\right)^{\frac{8}{3}} \sim 1$, and for $\hbar\omega \gg 1keV \quad \tau_x \to 0$.

When observing X-ray sources in the soft X-ray region ($\lesssim 1keV$) one has to take into account the absorption due to the interstellar gas and correct thus accordingly.

Chapter 4

Compton scattering

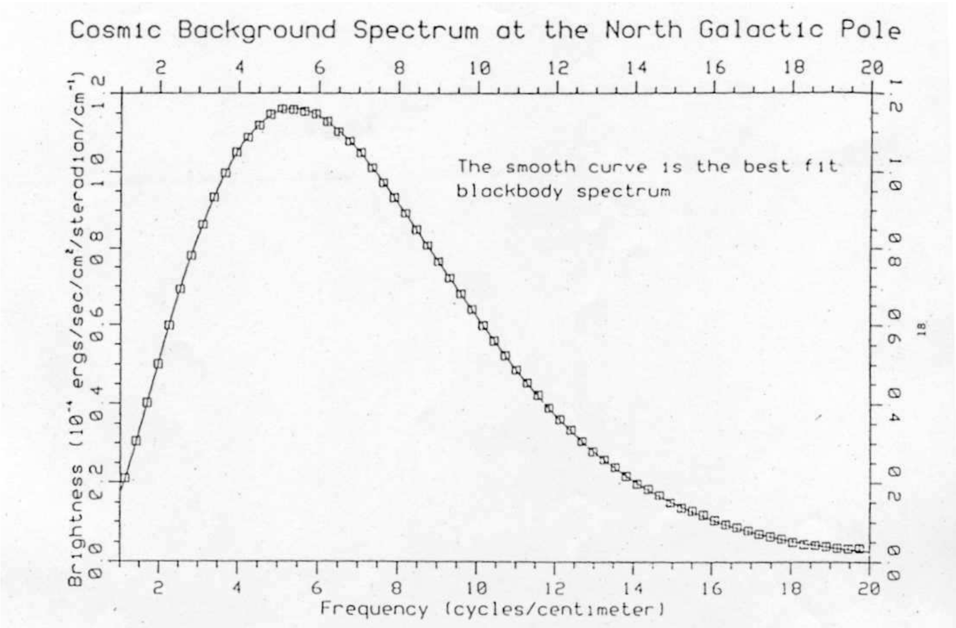

Figure 4.1: The spectrum of the Cosmic Microwave Background Radiation as measured by the COBE satellite in the direction of the North Galactic Pole. Within the quoted errors, the spectrum is that of a perfect black body. From Ref. [22]

In Compton scattering an incoming high energy photon scatters on an electron (assume it to be at rest) and thus a fraction of its momentum and energy is transferred to the electron. Therefore, the photons after the collision have less energy and momentum. Let's consider first Thomson scattering, which one gets as limiting case of Compton scattering for low energy photons, $\hbar\omega \ll m_e\, c^2$.

We will derive the formula for the scattering of an unpolarized beam of radiation (propagating into z direction as illustrated in Figure 4.2) upon a stationary

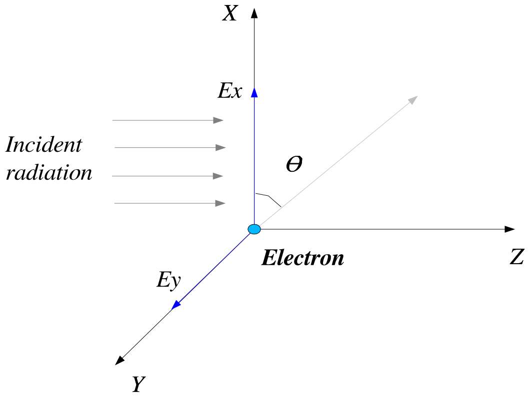

Figure 4.2: Geometry of Thomson scattering of a beam of radiation by a free electron .

electron.

The electric fields experienced by the electron (at the origin of the reference frame) in the x and y directions are:

$$E_x = E_{x_0}\, e^{i\omega t} \quad \text{and} \quad E_y = E_{y_0}\, e^{i\omega t} \ , \tag{4.1}$$

respectively. Accordingly the electron experiences an acceleration in these directions:

$$\ddot{r}_x = \frac{e\, E_x}{m_e} \quad \text{and} \quad \ddot{r}_y = \frac{e\, E_y}{m_e} \ . \tag{4.2}$$

The intensity of the radiation scattered through an angle θ into the solid angle $d\Omega$ is

$$-\left(\frac{dE}{dt}\right)_x d\Omega = \frac{e^2\, |\ddot{r}_x|\, sin^2\theta}{16\pi^2\, \epsilon_0\, c^3}\, d\Omega = \frac{e^4\, |E_x|^2\, cos^2\alpha}{16\pi^2\, m_e^2\, \epsilon_0\, c^3}\, d\Omega \ , \tag{4.3}$$

where $\alpha = \frac{\pi}{2} - \theta$. Notice that by integrating equation (4.3) over the solid angle $d\Omega = 2\pi\, sin\theta\, d\theta$ one gets $-\left(\frac{dE}{dt}\right)_{rad} = \frac{q^2\, |\, \ddot{\vec{r}}_0\, |^2}{6\pi\, \epsilon_0\, c^3}$, i.e. equation (2.1). We take the time average of E_x^2, which is $\bar{E}_x^2 = \frac{1}{2} E_{x_0}^2$, and sum over all infalling waves which contribute to the x component of the radiation, E_x. This way we consider the infalling energy per unit surface on the electron. This quantity is given by the Pointing vector:

$$\vec{S}_x = (\vec{E} \wedge \vec{H}) = c\, \epsilon_0\, E_x^2\, \vec{i}_z \ ,$$

$\vec{i}_z$ being a unit vector in the z direction. Its time averaged value is given by:

$$S_x = \sum_i c\, \epsilon_0\, \frac{E_{x_0}^2}{2} \ ,$$

where the sum is over the infalling photons.

Thus

$$-\left(\frac{dE}{dt}\right)_x d\Omega \;=\; \frac{e^4\; cos^2\alpha}{16\;\pi^2\; m_e^2\; \epsilon_0^2\; c^4}\; S_x\; d\Omega\;. \tag{4.4}$$

From the Figure 4.2 one sees that the radiation in the xz plane from the acceleration of the electron in the y direction corresponds to the scattering at $\theta = \frac{\pi}{2}$ and therefore the scattered intensity in the α direction is just given by equation (4.4) but with x replaced by y and $cos^2\alpha$ replaced by 1:

$$-\left(\frac{dE}{dt}\right)_y d\Omega \;=\; \frac{e^4}{16\;\pi^2\; m_e^2\; \epsilon_0^2\; c^4}\; S_y\; d\Omega\;.$$

The total infalling energy per unit surface is $S = S_x + S_y$, and for unpolarized radiation $S_x = S_y = \frac{S}{2}$. Thus the total scattered radiation into $d\Omega$ is just the sum of the intensities of the radiation scattered in the x and y directions:

$$-\left(\frac{dE}{dt}\right) d\Omega \;=\; \frac{e^4}{16\;\pi^2\; m_e^2\; \epsilon_0^2\; c^4}\left(1 + cos^2\alpha\right)\frac{S}{2} d\Omega\;. \tag{4.5}$$

The differential scattering cross-section $d\sigma_T$ is then given by:

$$d\sigma_T = \frac{r_e\;\left(1 + cos^2\alpha\right)}{2}\; d\Omega\;, \tag{4.6}$$

where $r_e = \frac{e^2}{4\pi\;\epsilon_0\; m_e\; c^2}$ is the classical electron radius[1].

The total cross-section is thus given by integrating over the solid angle $d\Omega = 2\pi\; sin\alpha\; d\alpha$, which leads to:

$$\sigma_T = \frac{8\pi}{3}\; r_e^2 = 6.65 \times 10^{-29}\; m^2\;, \tag{4.7}$$

which is the Thomson cross-section.

Assuming that the incident photon beam is along the x axis, the photons number density decrease is given by:

$$-\frac{dN}{dx} = \sigma_T\; N\; N_e\;, \tag{4.8}$$

with N being the number density of photons and N_e the number of electrons per unit volume. Thus the photon number density decreases exponentially:

$$N = N_0\; e^{-\int \sigma_T\; N_e\; dx}\;. \tag{4.9}$$

The *optical depth* τ is defined as

$$\tau = \int \sigma_T\; N_e\; dx\;. \tag{4.10}$$

[1] $\frac{d\sigma_T}{d\Omega}$ corresponds to the energy radiated per unit time per unit solid angle divided by the incident energy per unit time per unit area (i.e. S).

Accordingly the *mean free path* of the photon through the electron gas is defined as:

$$\lambda_e = (\sigma_T \, N_e)^{-1} \ . \tag{4.11}$$

In the Thomson scattering there is no change in the frequency of the radiation, which is a good approximation as long as $\hbar\omega \ll m_e \, c^2$.

However, when the photon scatters with an electron it loses energy and thus its wavelength increases. A detailed relativistic calculation gives the following result for the ratio of the frequencies before and after the scattering, ω and ω' respectively:

$$\frac{\omega'}{\omega} = \frac{1 - \beta \, cos\theta}{1 - \beta \, cos\theta' + \frac{\hbar\omega}{\gamma m_e c^2} \, (1 - cos\alpha)} \ , \tag{4.12}$$

where $\beta = \frac{v}{c}$, $\gamma = \left(1 - \beta^{\,2}\right)^{-\frac{1}{2}}$ is the Lorentz factor, with $\vec{v}$ the velocity of the electron, and α is the angle between the incoming and the outgoing wave-vectors of the photon, $\vec{k}$ and $\vec{k'}$ respectively, θ is the angle between $\vec{k}$ and $\vec{v}$ (the velocity of the electron before the scattering), and θ' is the angle between $\vec{k'}$ and $\vec{v'}$ (the velocity of the electron after the scattering).

For a stationary electron, i.e. $\vec{v} = 0$, $\gamma = 1$ and equation (4.12) reduces to:

$$\frac{\omega'}{\omega} = \frac{1}{1 + \frac{\hbar\omega}{\gamma m_e c^2} \, (1 - cos\alpha)} \ ,$$

or

$$\frac{\Delta\lambda}{\lambda} = \frac{\lambda' - \lambda}{\lambda} = \frac{\hbar\omega}{\gamma m_e c^2} \, (1 - cos\alpha) \ . \tag{4.13}$$

For energies of the photons comparable or bigger than the electron rest energy, i.e. $\hbar\omega \gtrsim m_e \, c^2$, one has to compute the cross-section using relativistic quantum mechanics. The relevant total cross-section is given by the Klein-Nishina formula:

$$\sigma_{KN} = \pi \, r_e^2 \, \frac{1}{\epsilon} \left[\left(1 - \frac{2\,(\epsilon + 1)}{\epsilon^2} \right) ln(2\epsilon + 1) + \frac{1}{2} + \frac{4}{\epsilon} - \frac{1}{2\,(2\epsilon + 1)^2} \right] \ , \tag{4.14}$$

where $\epsilon = \frac{\hbar\omega}{m_e \, c^2}$. For low energy photons, i.e. $\epsilon \ll 1$, equation (4.14) becomes

$$\sigma_{KN} = \frac{8\pi}{3} \, r_e^2 \ (1 - 2\epsilon) = \sigma_T \ (1 - 2\epsilon) \simeq \sigma_T \ ; \tag{4.15}$$

whereas in the ultrarelativistic regime, $\epsilon \gg 1$, it becomes

$$\sigma_{KN} = \pi \, r_e^2 \, \frac{1}{\epsilon} \left(ln2\epsilon + \frac{1}{2} \right) \ . \tag{4.16}$$

If the photons have low energy, whereas the electrons are ultrarelativistic, one gets the situation in which the photons acquire energy, instead of losing it. This process is called *inverse Compton scattering* because the electrons lose energy rather than the photons.

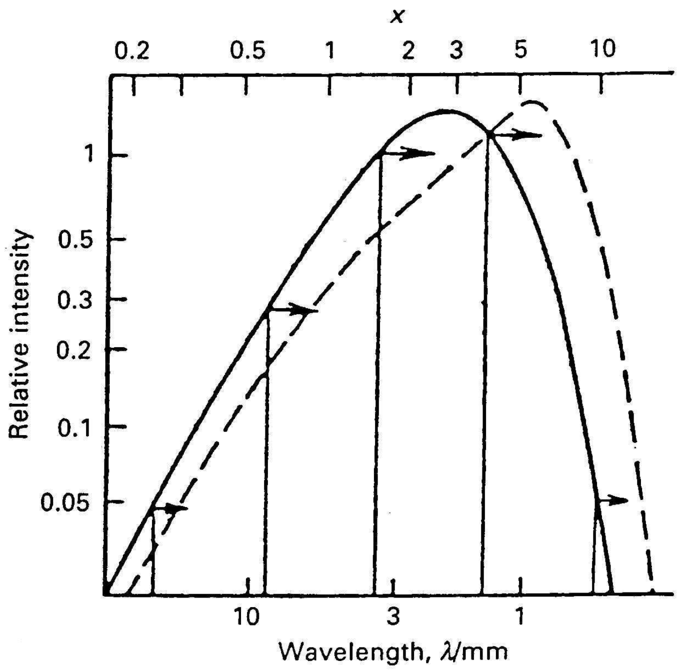

Figure 4.3: Illustrating the Compton scattering of a Planck distribution by hot electrons in the case in which the Compton optical depth $y = \int (kT_e/m_e c^2)\sigma_T N_e \, dl = 0.15$. The intensity decreases in the Rayleigh-Jeans region of the spectrum and increases in the Wien region. From Ref. [23]

If the energy of the photons in the centre of momentum frame is much smaller than $m_e\, c^2$ (i.e. $\gamma \hbar\omega \ll m_e\, c^2$), and thus the centre of momentum frame is very closely that of the relativistic electron, one can show that the energy loss rate of the electrons is given by:

$$\left(\frac{dE}{dt}\right) = \frac{4}{3}\, \sigma_T\, c\, u_{rad} \left(\frac{v^2}{c^2}\right) \gamma^2 \tag{4.17}$$

where u_{rad} is the energy density of the radiation ($u_{rad} = N\, \hbar\omega$).

The maximum energy which a photon can acquire in the inverse Compton scattering (corresponding to an head-on collision in which the photon is sent back along its original path) is

$$(\hbar\omega)_{max} = \hbar\omega_0\, \gamma^2 \left(1 + \frac{v}{c}\right)^2 \simeq 4\gamma^2\, \hbar\omega_0\ , \tag{4.18}$$

ω_0 being the photon frequency before the collision[2]. Typically the resulting frequency of a photon scattered by an ultrarelativistic electron is of order $\omega \sim \gamma^2\, \omega_0$. In various types of astronomical sources electrons are accelerated such that their Lorentz factor is $\sim 100 - 1000$.

Just as examples consider photons scattering on electrons with a Lorentz factor of 1000: radio photons with frequency $\nu_0 = 10^9\ Hz$ become ultraviolet photons, $\nu = 10^{15}\ Hz$, and optical photons, $\nu_0 = 4 \times 10^{14}\ Hz$, become γ-rays with frequency $\nu = 4 \times 10^{20}\ Hz$ (about 1.6 MeV).

Clearly the inverse Compton scattering process is a mean of producing very high energy photons. On the other hand this is also a way for ultrarelativistic electrons to lose energy whenever they go through a region in which there are many photons.

4.1 Comptonisation

Let's consider a hot thin plasma, as is the case for instance in the vicinity of X-ray binary sources, in the hot intergalactic gas in clusters of galaxies, or even in the primordial plasma in the early phases of the Big Bang. Photons which pass through such a medium will lose or acquire energy from the electrons. We consider the non-relativistic regime in which $k\, T_e \ll m_e\, c^2$ (T_e is the electron gas temperature) and $\hbar\omega \ll m_e\, c^2$. As seen in equation (4.12) the energy transferred to stationary electrons from the photons (if $\hbar\omega \ll m_e\, c^2$) is as follows:

$$\frac{\Delta\epsilon}{\epsilon} = \frac{\hbar\omega}{m_e\, c^2}\, (1 - cos\alpha)\ . \tag{4.19}$$

In the reference frame of the electron the scattering is simply Thomson scattering and the photons are isotropically distributed such that if we average over the

[2]The electrons are relativistic so $\frac{v}{c} \approx 1$.

scattering angle α we get:

$$< \frac{\Delta\epsilon}{\epsilon} > = \frac{\hbar\omega}{m_e\, c^2} \ , \tag{4.20}$$

since $< cos\alpha > = \int cos\alpha\ d\Omega = 0$.

On the other hand for the energy loss rate of high energy electrons in collision with low energy photons, taking the low energy limit of equation (4.17), one finds:

$$\left(\frac{dE}{dt}\right) = \frac{4}{3}\, \sigma_T\, c\, u_{rad}\, \left(\frac{v}{c}\right)^2 \ . \tag{4.21}$$

The number of scattered photons per second is equal to

$$\sigma_T\, N_{phot}\, c = \sigma_T\, u_{rad}\, \frac{c}{\hbar\omega_0} \ , \tag{4.22}$$

$\hbar\omega_0$ is the photon energy before the scattering.

Thus the average energy gain of the photons per Compton collision becomes

$$< \frac{\Delta\epsilon}{\epsilon} > = \frac{4}{3}\, \left(\frac{v}{c}\right)^2 \ , \tag{4.23}$$

obtained dividing equation (4.21) by equation (4.22) and putting $\epsilon = \hbar\omega_0$.

If the electrons have a thermal distribution of velocities at temperature T_e, then $\frac{1}{2}\, m_e < v^2 > = \frac{3}{2}\, k\, T_e$ and equation (4.23) reduces to

$$< \frac{\Delta\epsilon}{\epsilon} > = 4 \frac{k\, T_e}{m_e\, c^2} \ . \tag{4.24}$$

As a result the overall energy change of a photon is

$$\frac{\Delta\epsilon}{\epsilon} = -\frac{\hbar\omega_0}{m_e\, c^2} + 4 \frac{k\, T_e}{m_e\, c^2} \ . \tag{4.25}$$

Accordingly for $\hbar\omega_0 = k\, T_e$ there is no energy transfer between the photons and the electrons gas, whereas energy is transferred to the photons for $\hbar\omega_0 < 4\, k\, T_e$ and to the electrons for $\hbar\omega_0 > 4\, k\, T_e$.

The optical depth for Thomson scattering is $\tau_e = N_e\, \sigma_T\, l$ (if N_e is constant). If $\tau_e \gg 1$ then the photon will be scattered several times before leaving the region, more precisely it turns out that the number of scatterings is τ_e^2. Instead, if $\tau_e \ll 1$ the number of scatterings is just τ_e. Hence the condition for a significant distortion of the photon spectrum by inverse Compton scattering is that

$$\frac{\Delta\epsilon}{\epsilon} = 4 \frac{k\, T_e}{m_e\, c^2}\, max(\tau_e, \tau_e^2) \geq 1 \ .$$

An exact treatment of the description of how the photon spectrum gets modified through the scattering on electrons requires the use of the Boltzmann equation, whose solution is quite involved.

However, when the electrons are non-relativistic, the fractional energy transfer $\frac{\Delta\epsilon}{\epsilon}$ per scattering is small. The Boltzmann equation can then be expanded to the second order in this small quantity, leading to an approximation (the Fokker-Planck equation), which for photons scattering off a non-relativistic thermal distribution of electrons was first derived by Kompaneets (1957) [24] and is known as *Kompaneets equation*.

The Kompaneets equation is as follows:

$$\frac{\partial n}{\partial y} = \frac{1}{x^2}\,\frac{\partial}{\partial x}\left[x^4\,\left(n + n^2 + \frac{\partial n}{\partial x}\right)\right] \,, \tag{4.26}$$

where $n(\nu)$ is the photon occupation number at frequency ν, $x = \frac{h\nu}{kT}$ and

$$y = \int \frac{k\,T_e}{m_e\,c^2}\,\sigma_T\,N_e\,dl \,, \tag{4.27}$$

if T_e does not depend on the position then y is proportional to the optical depth τ.

The term $\partial n/\partial x$ represents the diffusion of photons along the frequency axis. The terms n and n^2 represent the cooling of the photons. One can easily verify that the term in the brackets in equation (4.26) vanishes for a Bose-Einstein distribution, for which the occupation number is $n = [\,exp\,(x+\mu) - 1\,]^{-1}$, where μ is the chemical potential. Then this is a solution of the Kompaneets equation for which $\partial n/\partial y = 0$. In general it has to be solved numerically.

An important application of the Kompaneets equation is the description of the distortions of the spectrum of the 2.7 K cosmic microwave background (CMB) radiation. There are two important cases:

i. If for some reason the intergalactic gas were heated to a very high temperature such that $T_e \gg T_r$ ($T_r = 2.7\ K$ is the CMB temperature), then the Compton scattering would increase the energy of the photons of the CMB. As a result there would be a deviation from Planck's distribution. If this process occurred instead in the early universe before the epoch of recombination, there would have been many scatterings and thus a new equilibrium would have been set up with a Bose-Einstein distribution with a non-vanishing chemical potential μ. In the previous situation, where the electrons have been heated up after recombination there would not be enough time to set up the equilibrium distribution and one would have to compute the spectrum according to the Kompaneets equation (4.26), but without the terms n and n^2 describing the cooling, since the photons cannot give away their energy:

$$\frac{\partial n}{\partial y} = \frac{1}{x^2}\,\frac{\partial}{\partial x}\left(x^4\frac{\partial n}{\partial x}\right) \,. \tag{4.28}$$

Zeldovich and Sunyaev have found a solution to this equation, which leads to:

$$\frac{\Delta u_\nu}{u_\nu} = y\,\frac{xe^x}{e^x - 1}\,\left[x\left(\frac{e^x+1}{e^x-1}\right) - 4\right] \,, \tag{4.29}$$

where

$$u_\nu = \frac{8\pi\, h\nu^3}{c^3}\left[e^{x+\mu} - 1\right]^{-1}$$

is the radiation energy density per frequency for a blackbody spectrum. The intensity of the CMB increases in the Wien region of the spectrum and decreases in the Rayleigh-Jeans region ($x \ll 1$), where using equation (4.29) one finds:

$$\frac{\Delta T}{T_r} = -2y\ . \tag{4.30}$$

COBE measurements have given the following constraints :

$$|\mu| < 9 \times 10^{-5}$$
$$y \lesssim 1.2 \times 10^{-5}$$

where y is the *Comptonisation* parameter.

ii. A second important application is the Compton scattering of photons of the CMB as they propagate to the Earth through regions of very hot ionised gas, as is in the case of clusters of galaxies which are embedded in an hot intracluster gas (*Sunyaev Zeldovich Effect* 1970) [25] [26].

As an example we consider the Coma cluster of galaxies:

$T_e \simeq 10^8\ K$ is the electron temperature, $N_e \simeq 3 \times 10^3\ m^{-3}$ is the electron density[3], $\sigma_T = 6.6 \times 10^{-29}\ m^2$, the core radius is $\sim 0.5\ Mpc$ and for the extension of the cluster we take a radius of $\sim 1\ Mpc$. With these values we find $y \simeq 0.9 \times 10^{-4}$ and accordingly $\Delta T/T_r \simeq -1.8 \times 10^{-4}$ in the Rayleigh-Jeans region.

This corresponds to a decrease of the temperature of the CMB of the order of $\Delta T \sim 0.1\ mK$ in the Rayleigh-Jeans part of the spectrum. These are difficult measurements, which are now performed by several groups on already a substantial amount of clusters.

From X-ray measurements one can determine the temperature and the electron density of a given cluster. From SZ measurements one can determine y and thus the size of the cluster. On the other hand the angular diameter is also inferred from the observations. Thus one can determine the angular distance of the cluster and then the Hubble constant.

If the cluster is moving with respect to the CMB rest frame there will be an additional spectral distortion due to the Doppler effect of the cluster bulk velocity on the scattered CMB photons. The so-called kinetic SZ is of the magnitude [26]:

$$\frac{\Delta T_{SZ}}{T_{CMB}} = -y\,\frac{v_{cluster}}{c}\ ,$$

where $v_{cluster}$ is the velocity component along the line of sight.

[3] or equivalently the proton density.

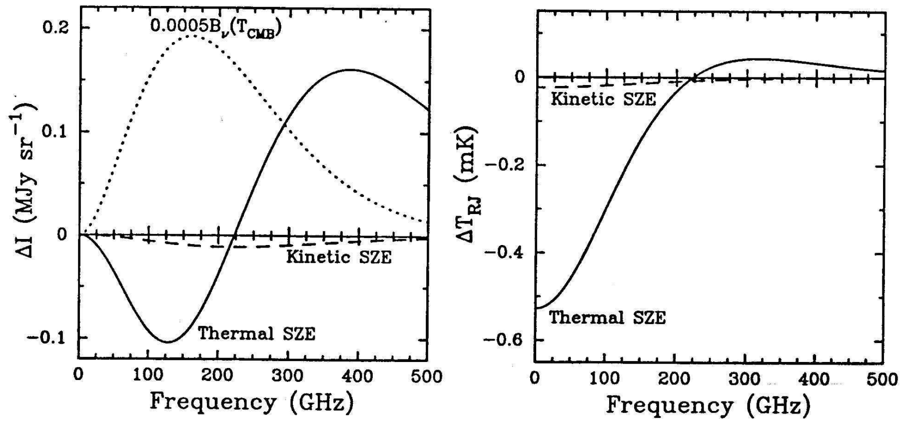

Figure 4.4: Spectral distortion of the cosmic microwave background (CMB) radiation due to the Sunyaev-Zeldovich effect (SZ). The left panel shows the Rayleigh-Jeans brightness temperature. The thick solid line is the thermal SZ and the dashed line is the kinetic SZE. For reference the 2.7 K thermal spectrum of the CMB intensity scaled by 0.0005 is shown by the dotted line in the left panel. The cluster properties used to calculate the spectra are an electron temperature of 10 keV, a Compton y parameter of 10^{-4}, and a peculiar velocity of 500 $km\ s^{-1}$. From Ref. [27]

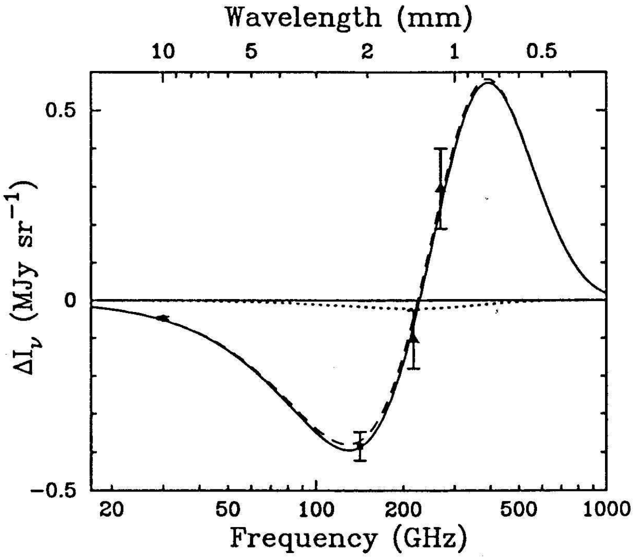

Figure 4.5: The measured SZ spectrum of Abell 2163. The data point at 30 GHz is from the Berkeley-Illinois-Maryland-Association (BIMA) array, at 140 GHz it is the weighted average of Diabolo and SuZIE measurements and at 218 GHz and 270 GHz from SuZIE. The best fit thermal and kinetic SZ spectra are shown by the dashed line and the dotted lines, respectively, with the spectra of the combined effect shown by the solid line. The limits on the Compton y-parameter and the peculiar velocity are $y_0 = 3.56^{+0.41+0.27}_{-0.41-0.19} \times 10^{-4}$ and $v_p = 410^{+1030+460}_{-850-440}\ km\ s^{-1}$, respectively, with statistical followed by systematic uncertainties at 68% confidence. From Ref. [27]

Chapter 5

Synchrotron radiation

The synchrotron radiation emitted by relativistic and ultrarelativistic electrons is one of the dominant processes in high energy astrophysics. It is the radiation emitted by very high energy electrons gyrating in a magnetic field. This mechanism is at the origin of the radio emission of our Galaxy, from supernova remnants and extragalactic sources. One refers to it also as non-thermal emission, which means that the spectrum cannot be described by a black body or a bremsstrahlung spectrum.

Consider a magnetic field $\vec{\mathcal{B}}$, uniform and static, an electron with velocity $\vec{v}$, moves according to the Lorentz equation:

$$\frac{d}{dt}(\gamma\, m_e\, \vec{v}) = e\, \left(\vec{v} \wedge \vec{\mathcal{B}}\right)\,, \tag{5.1}$$

where γ is the Lorentz factor. In a magnetic field the acceleration is always perpendicular to the velocity vector of the particle, then $\vec{a}_{\|} = 0$ and $d\gamma/dt = 0$. Thus equation (5.1) reduces to

$$\gamma\, m_e\, \frac{d\vec{v}}{dt} = e\, \left(\vec{v} \wedge \vec{\mathcal{B}}\right) = e\, v\, \mathcal{B}\, sin\alpha\, \vec{i}_{\perp}\,,$$

with $\vec{i}_{\perp}$ a unit vector perpendicular to $\vec{v}$ and α the angle between the magnetic field $\vec{\mathcal{B}}$ and the electron velocity $\vec{v}$. This way we get for the perpendicular component of the acceleration:

$$|\vec{a}_{\perp}| = \frac{e\, v\, \mathcal{B}\, sin\alpha}{m_e\, \gamma}\,. \tag{5.2}$$

Following equation (2.5) with $\vec{a}_{\|} = 0$, we get for the total radiation loss rate of the electron due to synchrotron radiation:

$$\begin{aligned} -\left(\frac{dE}{dt}\right) &= \frac{e^2\, \gamma^4}{6\pi\, \epsilon_0\, c^3}\, |a_{\perp}|^2 \\ &= \frac{e^2\, \gamma^4}{6\pi\, \epsilon_0\, c^3}\, \frac{e^2\, v^2\, \mathcal{B}^2\, sin^2\alpha}{m_e^2\, \gamma^2} \\ &= \frac{e^4\, \mathcal{B}^2}{6\pi\, \epsilon_0\, c\, m_e^2}\, \left(\frac{v}{c}\right)^2\, \gamma^2\, sin^2\alpha\,. \end{aligned} \tag{5.3}$$

With $\mathcal{U}_{mag} = \mathcal{B}^2/2\,\mu_0$ the energy density of the magnetic field, σ_T the Thomson cross-section and $c^2 = 1/\mu_0\epsilon_0$, equation (5.3) can also be written as:

$$-\left(\frac{dE}{dt}\right) = 2\,\sigma_T\,c\,\mathcal{U}_{mag}\,\left(\frac{v}{c}\right)^2\,\gamma^2\,sin^2\alpha\;. \tag{5.4}$$

This result is valid for an electron with a given angle α (called also the *pitch* angle). Assuming an isotropic distribution of pitch angles we can average over it, taking into account that the distribution is as follows[1]:

$$p\,(\alpha)\;\;d\alpha = \frac{1}{2}\,sin\alpha\,d\alpha\;,$$

and that the average is given by:

$$\int_0^\pi\;p\,(\alpha)\;\;sin^2\alpha\,d\alpha = \frac{1}{2}\int_0^\pi\;sin^3\alpha\;d\alpha = \frac{2}{3}\;,$$

we get for the radiation loss:

$$-\left(\frac{dE}{dt}\right) = \frac{4}{3}\,\sigma_T\,c\,\mathcal{U}_{mag}\,\left(\frac{v}{c}\right)^2\,\gamma^2\;. \tag{5.5}$$

During its lifetime an high energy electron is likely to be randomly scattered, and thus equation (5.5) is the correct expression for its average energy loss rate.

5.1 Synchrotron lifetime

For an ultrarelativistic electron ($\gamma^2 = \left(E/m_e\,c^2\right)^2$ and $v \simeq c$ such that $\frac{v}{c} \simeq 1$) equation (5.5) gets:

$$-\left(\frac{dE}{dt}\right) = \rho\,E^2\;, \tag{5.6}$$

with $\rho = \frac{4}{3}\,\sigma_T\,c\,\mathcal{U}_{mag}/m_e^2\,c^4$.

This equation can be solved and leads to

$$\left(\frac{1}{E}\right) = \rho t + const\;.$$

Let's assume that for $t = 0, E = E_0 \gg m_e\,c^2$, then

$$E\,(t) = \frac{E_0}{1 + \rho\,E_0\,t}\;. \tag{5.7}$$

After the time $t_{\frac{1}{2}} = \frac{1}{\rho\,E_0}$ the energy of the particle is half of its initial energy : $E\left(t_{\frac{1}{2}}\right) = \frac{E_0}{2}$.

[1] Notice that $\int_0^\pi\;p\,(\alpha)\;\;d\alpha = 1$.

Correspondingly

$$t_{\frac{1}{2}}\,[s] = \frac{5.1\times10^{8}}{(\mathcal{B}\,[Gauss])^{2}}\,\frac{m_e\,c^{2}}{E_0}\ . \tag{5.8}$$

We apply this result to the Crab nebula, which is the remaining of a supernova explosion which took place in the year 1054. The Crab nebula is a strong emitter of synchrotron radiation of about $10^{38}\ erg/s$, with a spectrum ranging from low radiofrequencies up to the γ-ray frequencies. The synchrotron spectrum is rather flat and decreases rapidly above a maximum frequency given by:

$$\nu_{max} = 0.07\,\frac{e\,\mathcal{B}}{m_e\,c}\left(\frac{E_0}{m_e\,c^{2}}\right)^{2}\ , \tag{5.9}$$

with a typical value of $\mathcal{B}_{\perp}\simeq 5\times10^{-4}\ Gauss$. Solving equation (5.9) for E_0 and substituting in equation (5.8), one finds the following expression for $t_{\frac{1}{2}}$:

$$t_{\frac{1}{2}}\,[s] = 6.1\times10^{11}\ \left(\mathcal{B}\,[Gauss]\right)^{-\frac{3}{2}}\ \left(\nu_{max}\,[Hz]\right)^{-\frac{1}{2}}\ . \tag{5.10}$$

For $\nu_{max}\simeq10^{20}\ Hz$ (and $\mathcal{B}\simeq 5\times10^{-4}\ Gauss$) we see that $t_{\frac{1}{2}}$ is about 10 weeks! Since the Crab nebula is now 949 years old, this means that the nebula is continuingly refurbished of ultrarelativistic electrons ejected by the pulsar itself, which lies in the centre of the nebula.

5.2 Spectral distribution of the synchrotron radiation

As next we compute the spectral distribution of the synchrotron radiation (see also chapter 14 in Jackson). Consider a current $\vec{j}\,(\vec{x},t)$ which generates an electric field which in the far (radiation) zone is given by:

$$\vec{\mathcal{E}} = \frac{1}{r}\,\frac{\vec{n}\wedge\left(\vec{n}\wedge\frac{\partial\vec{j}}{\partial t}\right)}{c^{2}}\ , \tag{5.11}$$

where $\vec{n}=\frac{\vec{x}}{r}$, with $r=|\vec{x}|$, is a unit vector directed towards the observer. For a point charge the current is given by

$$\vec{j}\,(\vec{x},t) = e\,\vec{v}\,(t)\ \delta^{3}\left(\vec{x}-\vec{z}\,(t)\right)\ ,$$

with $\vec{v}\,(t)=\dot{\vec{z}}\,(t)$.

The emitted radiation E_{rad} per unit time and solid angle $d\Omega$ is then

$$\frac{d^{2}E_{rad}}{d\Omega\,dt} = r^{2}\,\frac{c}{16\pi^{2}\,\epsilon_0}\,|\vec{\mathcal{E}}\,(t)\,|^{2}\ . \tag{5.12}$$

Accordingly the total emitted radiation per solid angle is:

$$\frac{dE_{rad}}{d\Omega} = r^{2}\,\frac{c}{16\pi^{2}\,\epsilon_0}\int_{-\infty}^{+\infty}|\vec{\mathcal{E}}\,(t)\,|^{2}\,dt\ . \tag{5.13}$$

Analogously to equation (2.7) one can apply Parseval's theorem, so that

$$\int_{-\infty}^{+\infty} |\vec{\mathcal{E}}\,(t)\,|^2\; dt = \int_{-\infty}^{+\infty} |\vec{\mathcal{E}}\,(\omega)\,|^2\; d\omega\ ,$$

where $\vec{\mathcal{E}}\,(\omega)$ is the Fourier transform of $\vec{\mathcal{E}}\,(t)$, defined similarly to equation (2.6). From the definition of the emitted radiation, $I\,(\omega) = dE_{rad}/d\omega$, following equations (2.8) and (2.9) we get in the same way[2]:

$$\frac{dI\,(\omega)}{d\Omega} = \frac{2\;r^2\;c}{16\pi^2\;\epsilon_0}\;|\vec{\mathcal{E}}\,(\omega)\,|^2\ . \tag{5.14}$$

Taking the Fourier transform of the current, $\vec{j}\,(\vec{x}, t)$:

$$\vec{j}\left(\vec{k}, \omega\right) = \frac{1}{2\pi}\int dt\; e^{i\omega t}\int d^3x\; e^{-i\vec{k}\cdot\vec{x}}\;\vec{j}\,(\vec{x}, t)\ \ ,$$

from equation (5.11) one gets:

$$|\vec{\mathcal{E}}\,(\omega)\,|^2 = \frac{1}{r^2}\,\frac{2\pi\;\omega^2}{c^4}\;|\vec{n}\wedge\vec{n}\wedge\vec{j}\left(\vec{k}, \omega\right)|^2\ , \tag{5.15}$$

which inserted in equation (5.14) gives:

$$\frac{dI\,(\omega)}{d\Omega} = \frac{1}{8\pi^2\;\epsilon_0}\,\frac{\omega^2}{c^3}\;2\pi\;|\vec{n}\wedge\vec{n}\wedge\vec{j}\left(\vec{k}, \omega\right)|^2\ . \tag{5.16}$$

For a pointlike charge, with $\vec{\beta} = \frac{\vec{v}}{c}$, the current has the following expression:

$$\begin{aligned}\vec{j}\left(\vec{k}, \omega\right) &= \frac{1}{2\pi}\int dt\; e^{i\omega t}\int d^3x\; e^{-i\vec{k}\cdot\vec{x}}\; e\;\vec{v}\,(t)\;\;\delta^3\left(\vec{x} - \vec{z}\,(t)\right)\\ &= \frac{e}{2\pi}\;c\int_{-\infty}^{+\infty} dt\; e^{i\omega t}\; e^{-i\vec{k}\cdot\vec{z}(t)}\;\vec{\beta}\,(t)\ \ ,\end{aligned}$$

then

$$\frac{dI\,(\omega)}{d\Omega} = \frac{e^2\;\omega^2}{16\pi^3\;\epsilon_0\;c}\;|\int_{-\infty}^{+\infty}\vec{n}\wedge\vec{n}\wedge\vec{\beta}\,(t)\,e^{i\omega\left(t - \frac{\vec{k}\cdot\vec{z}(t)}{\omega}\right)}\; dt\;|^2\ , \tag{5.17}$$

with $\frac{\vec{k}}{\omega} = \frac{\vec{n}}{c}$. Notice that the vector $\vec{n}\wedge\vec{n}\wedge\vec{\beta}$ points to the same direction as $\vec{\mathcal{E}}\,(t)$.

We evaluate now equation (5.17) for relativistic electrons. The particles rotate around the magnetic field lines at an angular frequency $\omega = e\mathcal{B}/\gamma m_e$ and with a pitch angle α with respect to the magnetic field direction. At any time the orbit has a certain radius ρ, which for instance at a given instant of time lies in the xy plane as in Figure 5.1. We put the origin of the reference frame at the point where the

[2] Notice that the factor 2 comes from the equality: $\int_{-\infty}^{+\infty}\;|\vec{\mathcal{E}}\,(\omega)\,|^2\; d\omega = 2\int_0^{\infty}\;|\vec{\mathcal{E}}\,(\omega)\,|^2\; d\omega$.

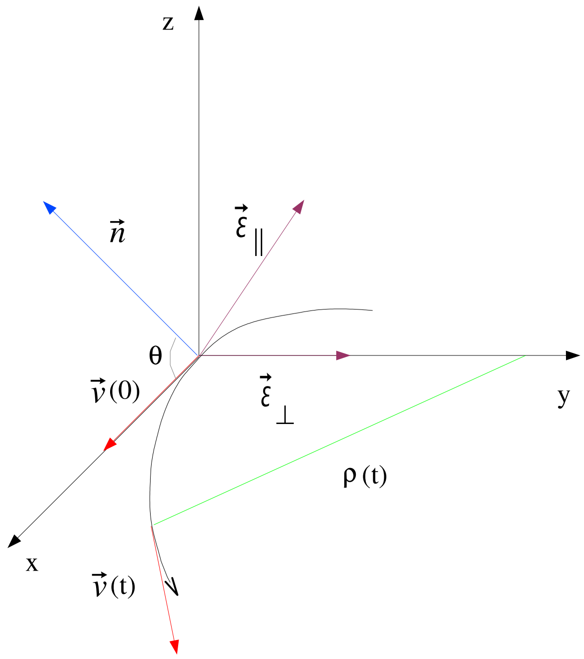

Figure 5.1: Geometry for evaluating the intensity and polarisation properties of synchrotron radiation. At $t = 0$ the particle velocity is along the x axis and ρ is the radius of curvature of the trajectory. From Ref. [1] and [10]

velocity vector $\vec{v}$ of the particle lies in the xz plane. The vector $\vec{n}$ pointing towards the observer lies also in the xz plane:

$$\vec{n} = (cos\ \theta, 0, sin\ \theta)\ ,$$

where θ is the angle between $\vec{n}$ and $\vec{v}$ at time $t = 0$. The y axis points then at $t = 0$ in the direction of the radius of the orbit, $\vec{\epsilon}_{\perp}$ lies on the y axis and $\vec{\epsilon}_{\parallel} = \vec{n} \wedge \vec{\epsilon}_{\perp}$. At time $t = 0$ the particle is sitting at the origin of the reference frame, whereas after a time t the particle has moved to a distance vt on the orbit, which can be parametrized as follows:

$$\vec{z}\,(t) = \left(\rho\ sin\frac{vt}{\rho}, \rho - \rho\ cos\frac{vt}{\rho}, 0\right)\ ,$$

whereas the corresponding velocity vector is ($\vec{\beta} = \vec{v}/c$);

$$\vec{\beta} = \left(\beta\ cos\frac{vt}{\rho}, \beta\ sin\frac{vt}{\rho}, 0\right)\ , \tag{5.18}$$

and thus

$$\vec{n} \wedge \left(\vec{n} \wedge \vec{\beta}\right) = -\beta\ sin\frac{vt}{\rho}\ \vec{\epsilon}_{\perp} + \beta\ cos\frac{vt}{\rho}\ sin\theta\ \vec{\epsilon}_{\parallel}\ .$$

We need to know these function only for very short periods of the order of ρ/vc as well as small angles $\theta \sim 1/\gamma$, so that we can make an expansion and get (with $v \simeq c$) :

$$\vec{n} \wedge \left(\vec{n} \wedge \vec{\beta}\right) \simeq -\frac{ct}{\rho}\,\vec{\epsilon}_{\perp} + \theta\,\vec{\epsilon}_{\parallel}\ . \tag{5.19}$$

To evaluate equation (5.17) we need moreover:

$$\begin{aligned}\omega t - \vec{k}\,\vec{z}\,(t) &= \omega\left[t - \frac{\vec{n}}{c}\cdot\vec{z}\,(t)\right]\\ &= \omega\left[t - \frac{\rho}{c}\,sin\frac{vt}{\rho}\,cos\theta\right]\\ &\simeq \omega\left[t - \beta t + \frac{\rho}{c}\,\frac{1}{6}\,\left(\frac{vt}{\rho}\right)^3 + \frac{\rho}{c}\,\frac{vt}{\rho}\,\frac{\theta^2}{2} + ...\right]\end{aligned}$$

which we expanded up to the third order in the small parameters θ and vt/ρ. Since $\beta = \sqrt{1-\gamma^2}$, $1-\beta \simeq \frac{1}{2\gamma^2}$ and by inserting, whenever possible, $\beta = 1$ we get:

$$\omega t - \vec{k}\,\vec{z}\,(t) \simeq \frac{\omega}{2}\,\left[\left(\frac{1}{\gamma^2}+\theta^2\right)t + \frac{c^2}{3\rho^2}\,t^3\right] \tag{5.20}$$

It is evident that the largest contributions come from the smallest values of the term in brackets in the exponential in equation (5.17). If this term would be large there would be many oscillations in the integral, which would average out to a very small value. Moreover synchrotron radiation is strongly beamed in the direction of motion of the electron. This implies that the main contribution comes from small values of θ and vt/ρ, thus justifying the approximation procedure.

Finally inserting equations (5.20) and (5.19) into equation (5.17) we find:

$$\frac{dI\,(\omega)}{d\Omega} \simeq \frac{e^2\,\omega^2}{16\pi^3\,\epsilon_0\,c}\,|-A_{\perp}(\omega)\,\vec{\epsilon}_{\perp} + A_{\parallel}(\omega)\,\vec{\epsilon}_{\parallel}|^2\ , \tag{5.21}$$

where

$$\begin{aligned}A_{\perp}(\omega) &= \frac{c}{\rho}\int_{-\infty}^{+\infty} t\,e^{\frac{i\omega}{2}\left[\left(\frac{1}{\gamma^2}+\theta^2\right)\,t+\frac{c^2}{3\,\rho^2}\,t^3\right]}dt\\ A_{\parallel}(\omega) &= \theta\int_{-\infty}^{+\infty} e^{\frac{i\omega}{2}\left[\left(\frac{1}{\gamma^2}+\theta^2\right)\,t+\frac{c^2}{3\,\rho^2}\,t^3\right]}dt\end{aligned} \tag{5.22}$$

Let's perform the following change of variables:

$$\eta = \frac{\omega\rho}{3c}\,\left(\frac{1}{\gamma^2}+\theta^2\right)^{\frac{3}{2}}$$

and introduce the new integration variable

$$x = \frac{ct}{\rho} \, \frac{1}{\sqrt{\frac{1}{\gamma^2} + \theta^2}} \, .$$

This way equations (5.22) become:

$$\begin{aligned} A_{\perp}(\omega) &= \frac{\rho}{c} \left(\frac{1}{\gamma^2} + \theta^2 \right) \int_{-\infty}^{+\infty} x \; e^{i \frac{3}{2} \eta \; \left(x + \frac{1}{3} x^3\right)} dx \\ A_{\|}(\omega) &= \frac{\rho \, \theta}{c} \left(\frac{1}{\gamma^2} + \theta^2 \right)^{\frac{1}{2}} \int_{-\infty}^{+\infty} e^{i \frac{3}{2} \eta \; \left(x + \frac{1}{3} x^3\right)} dx \, . \end{aligned} \tag{5.23}$$

Finally we find for equation (5.17):

$$\frac{dI\,(\omega)}{d\Omega} = \frac{e^2}{12 \pi^3 \, \epsilon_0 \, c} \left(\frac{\omega \rho}{c} \right)^2 \left(\frac{1}{\gamma^2} + \theta^2 \right)^2 \left[K_{\frac{2}{3}}^2 \,(\eta) + \frac{\theta^2}{\frac{1}{\gamma^2} + \theta^2} \, K_{\frac{1}{3}}^2 \,(\eta) \right] \, , \tag{5.24}$$

where we used the modified Bessel functions of order $2/3$ and $1/3$ respectively, which are defined as follows:

$$\begin{aligned} K_{\frac{2}{3}}^2 \,(\eta) &= \sqrt{3} \int_0^{\infty} x \; sin \left(\frac{3}{2} \eta \; \left(x + \frac{1}{3} x^3 \right) \right) \; dx \\ K_{\frac{1}{3}}^2 \,(\eta) &= \sqrt{3} \int_0^{\infty} cos \left(\frac{3}{2} \eta \; \left(x + \frac{1}{3} x^3 \right) \right) \; dx \, . \end{aligned} \tag{5.25}$$

In the limit cases $\eta \gg 1$ and $\eta \ll 1$ one can use the following asymptotic approximations of the modified Bessel functions:

$$\begin{aligned} &\eta \ll 1 \qquad K_{\nu}\,(\eta) \sim \frac{1}{2}\, \Gamma\,(\nu) \; \left(\frac{1}{2} \eta \right)^{-\nu} \; , \; \nu \neq 0 \\ &\eta \gg 1 \qquad K_{\nu}\,(\eta) \sim \sqrt{\frac{\pi}{2\eta}} \; e^{-\eta} \; \left(1 + \theta \left(\frac{1}{\eta} \right) \right) \, . \end{aligned} \tag{5.26}$$

Thus for $\eta \gg 1$ equation (5.24) decreases as $e^{-2\eta}$. From the definition of η one sees that η gets large for all angles θ if the frequency ω is large. Accordingly we can define a critical frequency requiring $2\eta = 1$ for $\theta = 0$. This gives:

$$\omega_c = \frac{3}{2} \, \gamma^3 \; \left(\frac{c}{\rho} \right) \, . \tag{5.27}$$

In the forward direction ($\theta = 0$) one gets the following approximate expressions for equation (5.17):

$$\left(\frac{dI\,(\omega)}{d\Omega}\right)_{\theta=0} \simeq \frac{e^2}{4\pi\,\epsilon_0\,c}\left[\frac{\Gamma\left(\frac{2}{3}\right)}{\pi}\right]^2 \left(\frac{3}{4}\right)^{\frac{1}{3}} \left(\frac{\omega\,\rho}{c}\right)^{\frac{2}{3}} \quad \text{for } \omega \ll \omega_c\,,$$

$$\left(\frac{dI\,(\omega)}{d\Omega}\right)_{\theta=0} \simeq \frac{3\,e^2}{8\pi^2\,\epsilon_0\,c}\,\gamma^2\left(\frac{\omega}{\omega_c}\right) e^{-\frac{\omega}{\omega_c}} \quad \text{for } \omega \gg \omega_c\,. \tag{5.28}$$

We see thus that for $\theta = 0$ the spectrum increases first as $\omega^{\frac{2}{3}}$, reaches a maximum for a value ω nearby ω_c and then decreases exponentially.

One can also give a crude estimate of the angular dependence (on θ) of equation (5.24) for a given frequency ω. We define, for a given frequency ω, the critical angle θ_c from the relation $\eta\,(\theta_c) = \eta\,(0) + 1$. For low frequencies ($\omega \ll \omega_c$ as defined by equation (5.27)) $\eta\,(0)$ is very small so that $\eta\,(\theta_c) \simeq 1$. Thus we get

$$\theta_c \simeq \left[\left(\frac{3c}{\omega\rho}\right)^{\frac{2}{3}} - \frac{1}{\gamma^2}\right]^{\frac{1}{2}} \simeq \frac{1}{\gamma}\left(\frac{2\,\omega_c}{\omega}\right)^{\frac{1}{3}} \quad \text{for } \omega \ll \omega_c\,, (\text{since } 1/\gamma^2 \ll 1). \tag{5.29}$$

On the other hand for $\omega \gg \omega_c$, $\eta\,(0) \gg 1$ and thus

$$\frac{dI}{d\Omega} \simeq \left(\frac{dI}{d\Omega}\right)_{\theta=0} e^{-\frac{3}{2}\gamma^2\theta^2\frac{\omega}{\omega_c}}\,, \tag{5.30}$$

where we used the expansion ($\left(1+\gamma^2\,\theta^2\right)^{\frac{3}{2}} \simeq 1 + \frac{3}{2}\gamma^2\,\theta^2 + ...$). For the critical angle $\theta_c \simeq \frac{1}{\gamma}\left(\frac{2\omega_c}{3\omega}\right)^{\frac{1}{2}}$ the spectral intensity decreases by $1/e$. One sees that at high frequencies the radiation is very much directed in the forward direction.

As next we integrate equation (5.24) over the solid angle to give the energy per frequency range radiated by the electron per complete orbit in the projected normal plane. During such an orbit the emitted radiation is almost completely confined to the solid angle which lies within an angle $\frac{1}{\gamma}$ of a cone of half-angle α, which is the pitch angle. Thus one can approximate the solid angle element by $d\Omega = 2\pi\,sin\alpha\,d\theta$ (i.e. to replace $sin\theta$ by $sin\alpha$). This way we find

$$I_\perp\,(\omega) = \frac{e^2\,\omega^2\,\rho^2\,sin\alpha}{6\pi^2\,\epsilon_0\,c^3\,\gamma^4}\int_{-\infty}^{+\infty}\left(1+\gamma^2\,\theta^2\right)^2\,K^2_{\frac{2}{3}}\,(\eta)\;d\theta$$

$$I_\parallel\,(\omega) = \frac{e^2\,\omega^2\,\rho^2\,sin\alpha}{6\pi^2\,\epsilon_0\,c^3\,\gamma^2}\int_{-\infty}^{+\infty}\left(1+\gamma^2\,\theta^2\right)^2\,\theta^2\,K^2_{\frac{1}{3}}\,(\eta)\;d\theta\,, \tag{5.31}$$

where the integration limits have been extended to $\pm\infty$ rather than $\pm\pi$. However since the integrand function is concentrated to small values of $\Delta\theta$ about α, the error in doing so is negligible. On the other hand this way it is possible to carry out the integration, such as to get

$$\begin{aligned} I_{\perp}(\omega) &= \frac{\sqrt{3}\, e^2\, \gamma\, sin\alpha}{8\pi\, \epsilon_0\, c}\, [F(x) + G(x)] \\ I_{\parallel}(\omega) &= \frac{\sqrt{3}\, e^2\, \gamma\, sin\alpha}{8\pi\, \epsilon_0\, c}\, [F(x) - G(x)]\ , \end{aligned} \tag{5.32}$$

where $x = \frac{\omega}{\omega_c}$ and ω_c is the critical angular frequency defined in equation (5.27) and the functions $F(x)$ and $G(x)$ are given in terms of modified Bessel functions:

$$\begin{aligned} F(x) &= x \int_x^{\infty} K_{\frac{5}{3}}(y)\ dy\ , \\ G(x) &= x\, K_{\frac{2}{3}}(x)\ , \end{aligned}$$

notice that $F(x)$ is maximal for $x \simeq 0.29$.

We recall that the radius of curvature, which enters in the definition of the critical angular frequency ω_c, is the one defined in the spiral orbit of the particle. However the plane containing the particle's orbit is inclined at a pitch angle α to the magnetic field. Therefore, with respect to the guiding centre of the particle's trajectory, the radius of curvature is $\rho = v/(\omega_r\, sin\alpha)$, $\omega_r = \omega_g/\gamma$ being the relativistic gyrofrequency, with $\omega_g = 2\pi\, \nu_g = \frac{e\mathcal{B}}{m_e}$ the non-relativistic gyrofrequency. This way we get

$$\omega_c = 2\pi\, \nu_c = \frac{3}{2}\left(\frac{c}{v}\right)\, \gamma^3\, \omega_r\, sin\alpha\ , \tag{5.33}$$

or $\nu_c = \frac{3}{2}\gamma^2\, \nu_g\, sin\alpha$, from which we see that most of the radiation is emitted at a frequency $\nu \simeq \gamma^2\, \nu_g$. Equation (5.32) represents the energy emitted in the two polarisations during one period of the electron in its orbit, which corresponds to the time $T_r = \nu_r^{-1} = 2\pi\, \gamma\, m_e/e\, \mathcal{B}$.

the total emissivity of a single electron by synchrotron radiation is the sum of the emissivity in the two polarisations divided by T_r:

$$j(\omega) = \frac{I_{\perp}(\omega)}{T_r} + \frac{I_{\parallel}(\omega)}{T_r} = \frac{\sqrt{3}\, e^3\, \mathcal{B}\, sin\alpha}{8\pi^2\, \epsilon_0\, c\, m_e}\, F(x)\ . \tag{5.34}$$

this is the spectral energy distribution, which has a broad maximum centered at the frequency $\nu = 0.29\, \nu_c$.

The total energy loss rate is thus given by

$$\begin{aligned} -\left(\frac{dE}{dt}\right) &= \int_0^{\infty} j(\omega)\ d\omega \\ &= \sigma_T\, c\, \mathcal{U}_{mag}\, \gamma^2\, sin^2\alpha\, \left(\frac{9\sqrt{3}}{4\pi}\right) \int_0^{\infty} F(x)\ dx\ . \end{aligned} \tag{5.35}$$

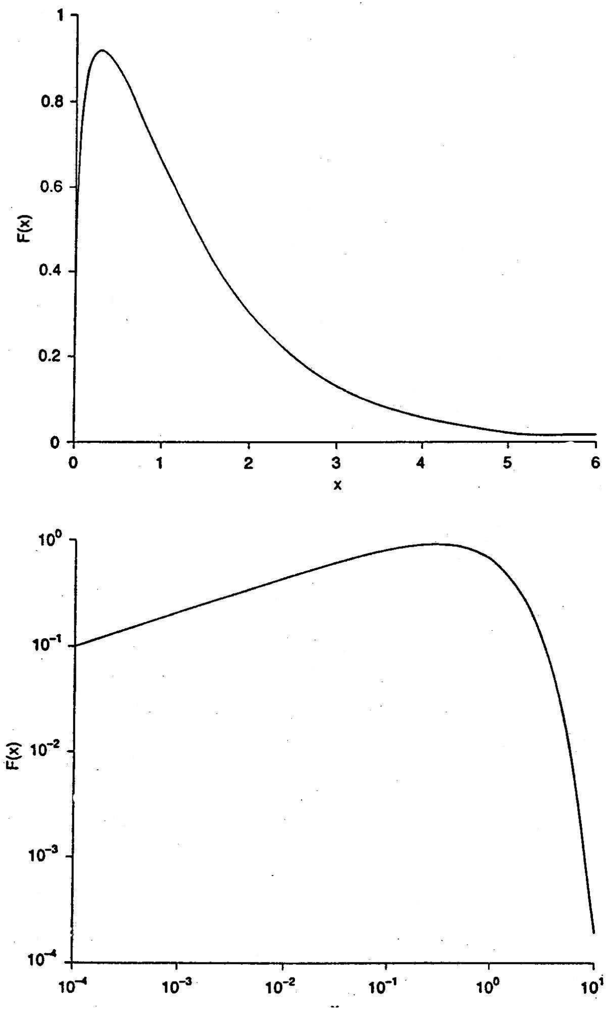

Figure 5.2: The intensity spectrum of the synchrotron radiation of a single electron shown (a) with linear axes and (b) with logarithmic axes. The function is plotted in terms of $x = \omega/\omega_c = \nu/\nu_c$, where ω_c is the critical angular frequency, $\omega_c = 2\pi\nu_c = \frac{3}{2}\left(\frac{c}{v}\right)\gamma^3\omega_r\ sin\alpha$. From Ref. [1]

The last integral can be performed to get:

$$\frac{9\sqrt{3}}{4\pi} \int_0^\infty F(x)\ dx = 2 \ .$$

Thus

$$-\left(\frac{dE}{dt}\right) = 2\,\sigma_T\, c\,\mathcal{U}_{mag}\,\gamma^2\, sin^2\alpha \ ,$$

which is exactly equation (5.4).

With the asymptotic expressions for $F(x)$, for $x \ll 1$ and $x \gg 1$, one gets the following expansions for $j(\omega)$:

$$j(\nu) \propto \nu^{\frac{1}{2}}\, e^{-\frac{\nu}{\nu_c}} \quad \text{for } x \gg 1 \quad (\nu \gg \nu_c) \ , \tag{5.36}$$

$$j(\omega) = \frac{e^2}{\sqrt[3]{3}\,\Gamma\left(\frac{1}{3}\right)\ 2\pi\,\epsilon_0\, c} \left(\frac{e\,\mathcal{B}\, sin\alpha}{\gamma\, m_e}\right)^{\frac{2}{3}} \omega^{\frac{1}{3}} \quad \text{for } x \ll 1 \quad (\omega \ll \omega_c) \ . \tag{5.37}$$

5.3 The synchrotron emission of a power-law distribution of electron energies

The energy spectra of cosmic rays and cosmic ray electrons can be approximated by power-law distributions of the form

$$N(E)\ dE = k\, E^{-p}\, dE \ , \tag{5.38}$$

where $N(E)\, dE$ is the number of electrons per unit volume in the energy interval $[E, E + dE]$, k being a constant. To get the emissivity of the electrons per unit volume we have to compute

$$\mathcal{J}(\omega) = \int_0^\infty j(x)\ k\, E^{-p}\, dE \ , \tag{5.39}$$

where $x = \frac{\omega}{\omega_c} = \frac{\omega}{\frac{3}{2}\,\gamma^2\,\omega_g\, sin\alpha} = \frac{2\omega\, m_e^2\, c^4}{3E^2\,\omega_g\, sin\alpha} \equiv \frac{A}{E^2}$. Thus $dE = -\frac{1}{2} A^{\frac{1}{2}} x^{-\frac{3}{2}} dx$, since $E = \sqrt{A/x}$, and therefore:

$$\begin{aligned} \mathcal{J}(\omega) &= \frac{k}{2\, A^{\frac{p-1}{2}}} \int_0^\infty j(x)\ x^{\frac{p-3}{2}}\, dx \qquad (5.40) \\ &= \frac{\sqrt{3}\, e^3\, \mathcal{B}\, k\, sin\alpha}{8\pi^2\,\epsilon_0\, c\, m_e\ (p+1)} \left(\frac{\omega\, m_e^3\, c^4}{3\, e\, \mathcal{B} sin\alpha}\right)^{-\frac{p-1}{2}} \Gamma\left(\frac{p}{4} + \frac{19}{12}\right) \Gamma\left(\frac{p}{4} - \frac{1}{12}\right) \ . \end{aligned}$$

As last point we have to integrate over the pitch angle α, for which we shall assume an isotropic distribution (clearly according to the application other distributions will be more appropriate and thus the results will change). An isotropic distribution means that α varies according to $\frac{1}{2}\, sin\alpha\, d\alpha$, and therefore with equation (5.40) we see that we have to carry out the integral:

$$\frac{1}{2}\int_0^{\pi} sin^{\frac{p+3}{2}}\alpha\, d\alpha = \frac{\sqrt{\pi}\,\Gamma\left(\frac{p+5}{4}\right)}{2\,\Gamma\left(\frac{p+7}{4}\right)} \,. \tag{5.41}$$

The emission per unit volume averaged over the pitch angle is thus given by

$$\begin{aligned} \mathcal{J}(\omega) = &\frac{\sqrt{3}\, e^2\, \mathcal{B}\, k}{16\pi^2\, \epsilon_0\, c\, m_e\ (p+1)} \left(\frac{\omega\, m_e^3\, c^4}{3\, e\, \mathcal{B}}\right)^{-\frac{p-1}{2}} \\ &\times \frac{\sqrt{\pi}\,\Gamma\left(\frac{p}{4}+\frac{19}{12}\right)\ \Gamma\left(\frac{p}{4}-\frac{1}{12}\right)\ \Gamma\left(\frac{p}{4}+\frac{5}{4}\right)}{\Gamma\left(\frac{p}{4}+\frac{7}{4}\right)} \,. \end{aligned} \tag{5.42}$$

The main dependences for the emissivity in the above formulae are

$$\mathcal{J}(\omega) \propto k\, \mathcal{B}^{\frac{p+1}{2}}\ \omega^{-\frac{p-1}{2}} \,, \tag{5.43}$$

we see that if the electron energy spectrum has power-law index p the spectral index of the synchrotron emission of these electrons is $\frac{p-1}{2}$.

5.4 The radio emission of the Galaxy

Once detailed radio maps of the Galaxy were made it was soon realized that it was essentially due to synchrotron radiation. The spectrum can be described (in the direction of the galactic north pole) as:

$$\begin{aligned} I(\nu) &\sim \nu^{-0.4} \qquad \text{for} \quad \nu \lesssim 200\ MHz \\ I(\nu) &\sim \nu^{-0.9} \qquad \text{for} \quad \nu \gtrsim 400\ MHz \,. \end{aligned}$$

This observed spectrum can be compared with the predicted spectrum assuming that the energy spectrum of cosmic ray electrons observed at the top of the Earth atmosphere is representative of the local interstellar medium as a whole. Below an energy $E < 10\ GeV$ the electron spectrum is strongly modulated by the Sun, whereas for $E > 10\ GeV$ it can be described as follows:

$$N(E)\ dE = 2.9 \times 10^{-5}\ E^{-3.3}\, dE\ \left[\frac{particles}{m^3\ sec}\right] \,. \tag{5.44}$$

Let's assume that this is representative for the ultrarelativistic electrons in the local interstellar medium. Electrons of energy $E = \gamma\, m_e\, c^2$ radiate most of their energy at a frequency $\nu \simeq 28\ \gamma^2\ \mathcal{B}\ GHz$, where $\mathcal{B}$ is measured in $Tesla$. Adopting an average local magnetic field strength $\mathcal{B} = 3 \times 10^{-10}\ \eta\, Tesla$ ($\eta \simeq 0.5 - 2$), then $10\ GeV$ electrons radiate most of their energy at a frequency $\nu \simeq 3.2\ \eta\ GHz$,

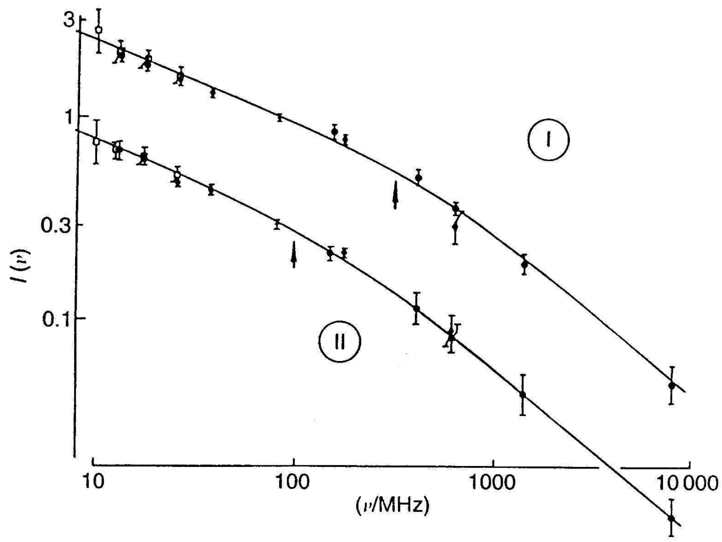

Figure 5.3: The spectrum of the Galactic radio emission. Region I corresponds to the anticentre direction at high galactic latitudes, and region II corresponds to the interarm region. From Ref. [28]

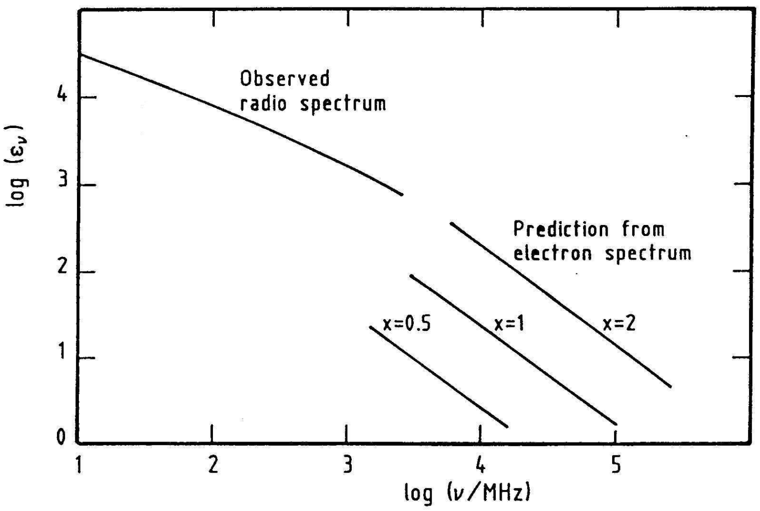

Figure 5.4: Comparison of the observed radio emissivity of the interstellar medium with that expected from the local electron energy spectrum for different values of the magnetic field strength. The radio emissivity is shown in relative units. The adopted radio emissivity at 10 MHz is 3×10^{-39} $W\ m^{-2}\ Hz^{-1}$. From Ref. [1]

which lies unfortunately just outside the range over which the galactic radio spectrum has been accurately measured. Therefore the best one can do is to find out if the predicted spectrum matches smoothly onto the observed galactic radio spectrum, since the synchrotron radiation spectrum of a power-law distribution of electrons energies is expected to be broad-band and smooth.

Inserting equation (5.44) into equations (5.42) or (5.43), we see that $p = 3.3$ and $\frac{p-1}{2} = 1.15$, thus

$$\mathcal{J}(\omega) \propto k\,(\eta\,\mathcal{B})^{2.15}\;\omega^{-1.15}\;.$$

By varying η one can get quite a good qualitative agreement with the observations. The assumption that the electrons can be described by the local measured spectrum can be checked as well and has to be somewhat modified.

5.5 Synchrotron emission of Radiogalaxies

In 1954 Baade and Minkowski identified the radioemitting source *Cygnus A* as being due to the brightest galaxy in a cluster of galaxies with redshift $z = 0.057$. This way they found that the luminosity in the radio band corresponded to about $L \sim 10^{45}\;erg/s$, which is 10^7 more than a typical galaxy emission in the radio and about 10 times the total optical luminosity of a galaxy. Early radio interferometer observations established then the extended nature of *Cygnus A* source, in form of a double structure about a central elliptical galaxy. This behaviour is quite common with a central galaxy or a quasar. These radio lobes are the result of gigantic jets of relativistic particles ejected from the central galaxy. These particles collide then with the intergalactic medium and also loose energy through interactions with the magnetic field present in the lobes, then producing synchrotron radiation in the radio band. Again the synchrotron age is short compared to the age of the radiosource, requiring thus a continuous supply of relativistic electrons from the radiogalaxy itself.

As next we estimate the energy content of a radiogalaxy, by evaluating the minimal energy content in form of relativistic particles and stored in the magnetic field.

For electrons we assume a power-law distribution as given in equation (5.38)

$$N(E) = k\,E^{-p}\;,$$

valid in the energy range $E_1 \le E \le E_2$. The total kinetic energy of the electrons is then:

$$E_e = \int_{E_1}^{E_2} E\,N(E)\;dE = k\int_{E_1}^{E_2} E^{-p+1}\,dE\;. \tag{5.45}$$

On the other hand the total synchrotron luminosity L due to the electrons [3] is given

[3]The radiation loss of a single electron is given by equation (5.4), where we put $\mathcal{B}\;sin\alpha = \mathcal{B}_\perp$ for the transverse component of the magnetic field, thus the radiation loss can be written as $const\;\mathcal{B}_\perp^2\;E^2$, where the constant can be inferred from equation (5.4).

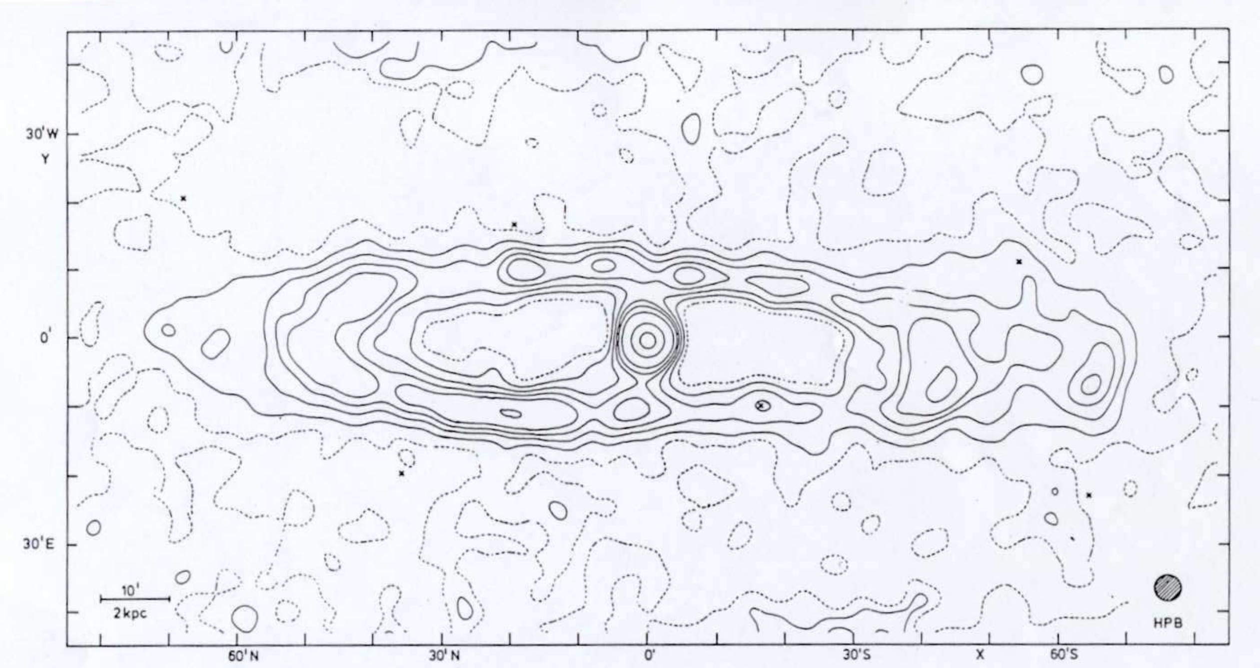

Figure 5.5: The distribution of synchrotron radio emission from nearby normal galaxies. In the Andromeda galaxy (M31, NGC 224), the synchrotron radio emission originates from a ring of emission with no central concentration of the radio emission, as in our Galaxy. There is a weak diffuse source in the central regions. From Ref. [29]

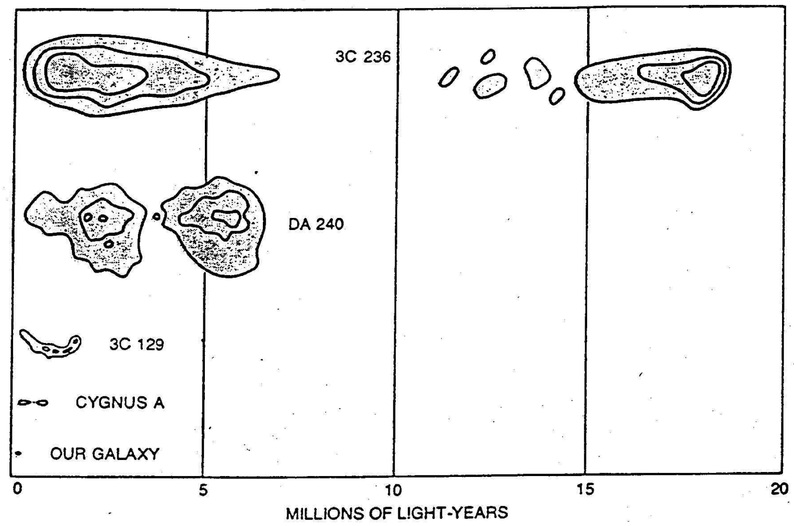

Figure 5.6: Extension of the radiolobes of some galaxies and quasars.

by:

$$\begin{aligned} L &= \int_{E_1}^{E_2} const\, \mathcal{B}_\perp^2\, E^2\, N(E)\, dE \\ &= const\, \mathcal{B}_\perp^2\, k \int_{E_1}^{E_2} E^{-p+2}\, dE\, . \end{aligned} \tag{5.46}$$

Moreover the values of E_1 and E_2 can be expressed through the critical frequency as given in equation (5.33)[4]. Finally we get:

$$E_e = \bar{C}\, \left(p, \omega_{c_1}, \omega_{c_2}\right)\, L\, \mathcal{B}^{-\frac{3}{2}}\, , \tag{5.47}$$

where $\bar{C}$ depends on p, ω_{c_1} and ω_{c_2}.

From the observations (by measuring $\mathcal{J}(\omega)$ in equation (5.42)) one gets p, ω_{c_1}, ω_{c_2}, L and thus E_e.

The total energy stored in the radio lobes (particles and magnetic field) is given by:

$$E_{tot} = E_e + E_p + E_{\mathcal{B}}\, , \tag{5.48}$$

where E_e is given by equation (5.47), $E_{\mathcal{B}} = \frac{\mathcal{B}^2}{8\pi}\, V$ is the magnetic energy (V being the volume of the radio lobes filled with a magnetic field), E_p is the energy of protons and other heavy particles which we assume to be proportional to E_e ($E_p = \bar{k}\, E_e$ with $1 \lesssim \bar{k} \lesssim 10^3$. This way the total energy becomes

$$E_{tot} = \left(1 + \bar{k}\right)\, \bar{C}\, L\, \mathcal{B}^{-\frac{3}{2}} + \frac{\mathcal{B}^2}{8\pi}\, V\, . \tag{5.49}$$

The magnetic field strength is unknown, so the best way to evaluate it is to minimize the total energy as a function of $\mathcal{B}$. Note that this value (sometimes called equipartition field) is not a minimum value for the magnetic field but that which leads to the lowest total energy.

The minimum of equation (5.49) leads to:

$$E_{\mathcal{B}} = \frac{3}{4}\, \left(1 + \bar{k}\right)\, E_e\, ,$$

which inserted into the expression for the magnetic energy gives:

$$\mathcal{B} \propto \left(\frac{L}{V}\right)^{\frac{2}{7}}\, ,$$

and

$$E_{tot}^{(min)} \propto L^{\frac{4}{7}}\, V^{\frac{3}{7}}\, .$$

[4]Where $\omega_{c_i} \propto \mathcal{B}_\perp\, E_i^2$ with $i = 1, 2$ and $\gamma^2 \simeq \left(E/mc^2\right)^2$.

As an example we consider the radio emission in the *Fornax A*, for which the observations give a value $p = 0.75$ for the spectrum in between $\nu_1 \sim 10^7\ Hz$ and $\nu_2 \sim 10^{10}\ Hz$. In that range the luminosity in the radioband is $L = 2.8 \times 10^{41}\ erg/s$. The estimated emission volume is $V = 2.2 \times 10^{70}\ cm^3$ and assuming $\bar{k} = 100$ one finds:

$$
\begin{aligned}
E_{tot}^{(min)} &\simeq 1.3 \times 10^{59}\, erg \\
\mathcal{B}^{(min)} &\simeq 8 \times 10^{-6}\, Gauss\ .
\end{aligned}
$$

The frequency interval corresponds for synchrotron emission to an energy range of the electrons between $280\ MeV$ and $9\ GeV$, assuming $\mathcal{B} = \mathcal{B}^{(min)}$.

The density of the electrons is of the order $10^{-10}\ cm^{-3}$ and then lifetime of $9\ GeV$ electrons in an $8\ mGauss$ magnetic field is about $t_{\frac{1}{2}} \sim 1.4 \times 10^7\ years$, thus relatively short. One sees that there is the problem of the production of the huge amount of energy which is possibly originated in a central supermassive black hole.

Chapter 6

The diffusion-loss equation for high energy electrons

Here we will study how the various energy loss processes discussed in the previous chapters will affect the spectrum of high energy electrons as they propagate from their source through the interstellar medium.

The following equation describes the energy spectrum and particles density at different points in the interstellar medium in the presence of continuous energy losses and supply of new particles from sources:

$$\frac{dN(E)}{dt} = \frac{d}{dE}\left[b(E)\ N(E)\right] + Q(E,t) + D\,\Delta N(E)\ , \tag{6.1}$$

D is a scalar diffusion coefficient, $N(E)$ is the number of particles per unit volume in the energy range $E, E + dE$, $Q(E,t)$ is the injection rate per unit volume of new particles (for instance coming from supernovae). The particles (electrons) within a certain volume overcome to energy gains and losses which can be written as follows:

$$-\left(\frac{dE}{dt}\right) = b(E)\ , \tag{6.2}$$

thus $b(E)$ stands for the energy loss by bremsstrahlung (equation (2.18)), Compton or inverse Compton effect (equation (4.17)) or synchrotron radiation (equation (5.5)).

The first term on the right hand side of equation (6.1) describes the fact that due to energy losses the particles in the energy range $E, E + dE$ get shifted to another energy range and replaced by other particles, which where before in another range. The second term describes the injection of new particles and the third term the diffusion. Equation (6.1) is also known as *diffusion-loss equation* for relativistic electrons. It is possible to solve equation (6.1) for a given distribution of sources and boundary conditions [30]. Here we will just mention a special case valid when considering steady state solutions ($\frac{dN}{dt} = 0$). For an infinite, uniform distribution of sources each injecting electrons with a spectrum $Q(E,t) = k\ E^{-p}$

one finds that if bremsstrahlung dominates $N(E) \sim E^{-p}$, that is the spectrum stays unchanged, whereas if inverse Compton effect or synchrotron losses dominate $N(E) \propto E^{-(p+1)}$, the spectrum gets steeper by one power of E.

Chapter 7

Acceleration of high energy particles

One of the most important and to a large extent still open problem in astrophysics is the mechanism by which high energy particles are accelerated to ultrarelativistic energies. In the following we will only briefly discuss the classical Fermi acceleration mechanism, since in the meantime this subject has become quite involved and a throughout treatment is beyond the scope of these notes.

The Fermi mechanism was first proposed by Fermi in 1949 [31] as a stochastic means by which particles colliding with clouds in the interstellar medium could be accelerated to high energies. In the original picture charged particles are reflected from *magnetic mirrors* associated with irregularities in the galactic magnetic field, or from massive clouds.

Consider thus a collision of a particle with a massive cloud, so that the velocity of the latter remains unchanged. The angle between the initial direction and the normal to the surface is θ. The centre of momentum frame coincides with that of the cloud (as it is infinitely massive) moving at velocity V.

In that frame the particle's energy in the collision is conserved, but in the observer's frame the energy E' of the particle after the collision is given by:

$$E' = \gamma^2 \, E \left[1 + \frac{2\, V \, v \, cos\theta}{c^2} + \left(\frac{V}{c}\right)^2 \right] \,, \tag{7.1}$$

where E and v are respectively the energy and the velocity in the observer frame before the collision and $\gamma = \left(1 - \frac{V^2}{c^2}\right)^{-1/2}$. Expanding the previous equation to the second order in $\frac{V}{c}$ one gets:

$$\frac{E' - E}{E} \equiv \frac{\Delta E}{E} = \frac{2\, V \, v \, cos\theta}{c^2} + 2\left(\frac{V}{c}\right)^2 \,. \tag{7.2}$$

As next we have to average over θ. The probabilities of head-on and following collisions are proportional to the relative velocities of approach of the particle and the cloud, namely $v + V\ cos\theta$ and $v - V\ cos\theta$, respectively. In the following we will assume $v \simeq c$ (relativistic particles) and thus the probabilities are proportional to $1 + (V/c)\ cos\theta$, where $0 \leq \theta \leq \pi$.

Moreover the probability that the pitch angle θ lies between θ and $\theta + d\theta$ is proportional to $sin\theta\ d\theta$, with $x = cos\theta$, we find (in the limit $v \to c$) that the angular average over the first term in equation (7.2) becomes

$$< \frac{2\ V\ cos\theta}{c} >= \left(\frac{2\ V}{c}\right) \frac{\int_{-1}^{+1} x\ \left(1 + \frac{V}{c} x\right)\ dx}{\int_{-1}^{+1} \left(1 + \frac{V}{c} x\right)\ dx} = \frac{2}{3} \left(\frac{V}{c}\right)^2 .$$

Thus in the relativistic limit the average energy gain per collision is

$$< \frac{\Delta E}{E} >= \frac{8}{3} \left(\frac{V}{c}\right)^2 . \qquad (7.3)$$

Thus the famous Fermi result tells that the average increase in energy is only of the second order in $\frac{V}{c}$. This result leads to an exponential increase in the energy of the particle since the same fractional increase occurs at each collision.

If the mean free path between clouds along a field line is λ, than the average (over angles) time between collisions turns out to be $t_{coll} = 2\lambda/c$

Therefore the typical rate of energy increase is given by

$$\frac{dE}{dt} = \frac{\Delta E}{t_{coll}} = \frac{4}{3} \left(\frac{V^2}{c\,\lambda}\right)\ E \equiv \alpha\ E\ . \qquad (7.4)$$

Let's assume that the particle remains in the accelerating region for a characteristic time τ_{esc}, we have then to add a term $-\frac{N(E)}{\tau_{esc}}$ on the right hand side of equation (6.1).

Suppose we are interested in the steady state solution of the so modified equation (6.1), thus $dN/dt = 0$, and moreover we assume that there is no source, $Q(E) = 0$, and no diffusion. The energy loss term is $b(E) = -\frac{dE}{dt} = -\alpha\ E$ (here it is an energy increase). This way we get the following equation

$$-\frac{d}{dE} \left[\alpha\ E\ N\left(E\right)\right] - \frac{N\left(E\right)}{\tau_{esc}} = 0\ , \qquad (7.5)$$

which leads to

$$\frac{dN\left(E\right)}{dE} = -\left(1 + \frac{1}{\alpha\ \tau_{esc}}\right) \frac{N}{E}\ ,$$

or

$$N\left(E\right) = const\ E^{-x}\ ,$$

where $x = 1 + (\alpha\ \tau_{esc})^{-1}$.

We thus see that the so obtained spectrum is a power-law, as confirmed afterwards by the observations.

Clearly the above derivation is oversimplified, nevertheless more detailed calculations lead also to power-law solutions [32].

Appendix

- ## Some useful definitions and formulae

  - **Energy conversion factors:**

$$E = h\nu = \frac{hc}{\lambda} = \frac{1.2399}{\lambda} = 4.136 \times 10^{-15}\ \nu\ eV$$
$$(\lambda \text{ in } \mu m = 10^{-6}\ m \text{ and } \nu \text{ in } Hz)$$

$$1\ eV = 1.602 \times 10^{-19}\ Joule = 1.602 \times 10^{-12}\ erg$$

$$\begin{aligned} E = kT &= 1.380 \times 10^{-23}\ T\ Joule \\ &= 8.617 \times 10^{-5}\ T\ eV \\ &\qquad (T \text{ in } Kelvin) \end{aligned}$$

- ## Astronomical wavebands

  - **Radio waveband :**

$$\begin{aligned} 3 \times 10^{6}\ Hz \leq \nu \leq 3 \times 10^{10}\ Hz \\ (3\ MHz \leq \nu \leq 30\ GHz) \\ 100\ m \geq \lambda \geq 1\ cm \end{aligned}$$

  - **Millimetre and sub-millimetre waveband :**

$$\begin{aligned} 3 \times 10^{10}\ Hz \leq \nu \leq 3 \times 10^{12}\ Hz \\ (30\ GHz \leq \nu \leq 3000\ GHz) \\ 10\ mm \geq \lambda \geq 0.1 mm \end{aligned}$$

- **Infrared waveband :**

$$3 \times 10^{12}\ Hz \leq \nu \leq 3 \times 10^{14}\ Hz$$
$$100\ \mu m \geq \lambda \geq 1\ \mu m$$

- **Optical waveband :**

$$3 \times 10^{14}\ Hz \leq \nu \leq 10^{15}\ Hz$$
$$1\ \mu m \geq \lambda \geq 300\ nm$$
$$(10000\ \mathring{A} \geq \lambda \geq 3000\ \mathring{A})$$

- **Ultraviolet waveband :**

$$10^{15}\ Hz \leq \nu \leq 3 \times 10^{16}\ Hz$$
$$300\ nm \geq \lambda \geq 10\ nm$$

- **X-ray waveband :**

$$3 \times 10^{16}\ Hz \leq \nu \leq 3 \times 10^{19}\ Hz$$
$$10\ nm \geq \lambda \geq 0.01\ nm$$
$$(100\ \mathring{A} \geq \lambda \geq 0.1\ \mathring{A})$$
$$0.1\ keV \leq E \leq 100\ keV$$

- **γ-ray waveband :**

$$\nu \geq 3 \times 10^{19}\ Hz$$
$$\lambda \leq 0.01\ nm\ (0.1\ \mathring{A})$$
$$E \geq 100\ keV$$

Acknowledgements

I would like to thank Prof. Martin Pohl for inviting me to give these lectures at the Troisième Cycle de la Physique en Suisse Romande.

I am especially grateful to Mrs. Mercedes Paniccia for her assistance in the lectures and for her help in preparing these notes and for several suggestions to improve them.

Thanks are also due to Rocco Piffaretti for some notes on galaxy clusters.

Bibliography

[1] M.S. Longair. *High Energy Astrophysics*, volume I and II. Cambridge University Press, 1992. and references therein.

[2] T.K. Gaisser. *Cosmic Rays and Particle Physics*. Cambridge University Press, 1990.

[3] Kenneth Greisen. End to the cosmic ray spectrum? *Phys. Rev. Lett.*, 16:748–750, 1966.

[4] G. T. Zatsepin and V. A. Kuzmin. Upper limit of the spectrum of cosmic rays. *JETP Lett.*, 4:78–80, 1966.

[5] M.S. Longair. In P.C. Davies, editor, *The new physics*. Cambridge University Press, 1988.

[6] R.G. Kron A.R. Sandage and M.S. Longair. *The Deep Universe*. Springer Verlag, 1995. Saas-Fee Lecture Notes.

[7] R. Giacconi. The Einstein X-ray Observatory. *Scientific American*, 242 num 2:80–102, February 1980.

[8] P.A. Charles and F.D. Seward. *Exploring the X-ray Universe*. Cambridge University Press, 1995.

[9] P. V. Ramana Murthy and A. W. Wolfendale. *Gamma-ray Astronomy*. Cambridge, UK: Univ. Pr., 1986.

[10] G.B. Rybicki and A.P. Lightman. *Radiative processes in Astrophysics*. John Wiley and Sons (New York), 1979.

[11] M. J. Henriksen and R. F. Mushotzky. *Astrophys. J.*, 302:287, 1986.

[12] R. Mushotzky. *X-ray astronomy*. R. Giacconi and G. Setti, page 174, Dordrecht:D. Reidel Publishing Co., 1980.

[13] C.L. Sarazin. *X-ray emission from clusters of galaxies*. Cambridge Astrophysics Series, 1988. available online at http://nedwww.ipac.caltech.edu/level5/March02/Sarazin/Sarazin_contents.html.

[14] R. Giacconi et al. *Astrophys. J.*, 178:281, 1972.

[15] J.E. Felten et al. *Astrophys. J.*, 146:955, 1966.

[16] V. Rephaeli. *Astrophys. J.*, 212:608, 1977.

[17] V. Rephaeli. *Astrophys. J.*, 218:323, 1977.

[18] A.C. Fabian et al. *Nature*, 263:301, 1976.

[19] A. Cavaliere and R. Fusco-Femiano. *Astron. and Astrophys.*, 49:137, 1976.

[20] R. H. Brown and R. J. Gould. *Phys. Rev.*, D1:2252, 1970.

[21] M. V. Zombeck. *Handbook of space astronomy and astrophysics*, pages 295–8. Cambridge University Press, 1990.

[22] J. C. Mather et al. *Astrophys. J.*, 354:L37, 1990.

[23] R. A. Sunyaev. *Soviet Astronomy Letters*, 6:213, 1980.

[24] A.S. Kompaneets. *Sov. Phys. JETP*, 4:730, 1957.

[25] R. A. Sunyaev and Ya. B. Zeldovich. *Comm. Astrophys. Space Phys.*, 4:173, 1972.

[26] R. A. Sunyaev and Ya. B. Zeldovich. *Mont. Not. R. Astron. Soc.*, 190:413, 1980.

[27] J. E. Carlstrom et al. *Ann. Rev. Astronom. Astrophys.*, 40:643, 2002.

[28] A.S. Webster. *Mon. Not. R. Astron. Soc.*, 166:355, 1974.

[29] J. E. V. Bystedt et al. *Astron. Astrophys. Suppl.*, 56:245, 1984.

[30] V.L Ginzburg and S.I. Syrovatskii. *The origin of cosmic rays*. Oxford Pergamon Press, 1964.

[31] E. Fermi. *Phys. Rev.*, 75:1169, 1949.

[32] V.S. Berezinskii et al. *Astrophysics of cosmic rays*. North-Holland, 1990.